

**STUDY OF SINGLE-PHASE FLOW IN STRUCTURED
PACKING USING COMPUTATIONAL FLUID
DYNAMICS**

By

SWAPNIL Y. DHUMAL

Bachelor of Technology

Laxminarayan Institute of Technology

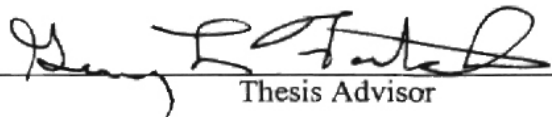
Nagpur University, India

2001

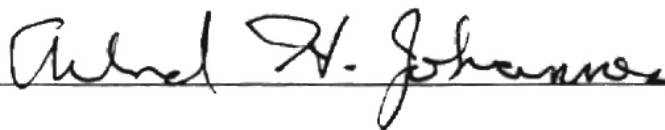
Submitted to the Faculty of the
Graduate College of the
Oklahoma State University
in partial fulfillment of
the requirements for
the Degree of
MASTER OF SCIENCE
August, 2003


**STUDY OF SINGLE-PHASE FLOW IN STRUCTURED
PACKING USING COMPUTATIONAL FLUID
DYNAMICS**

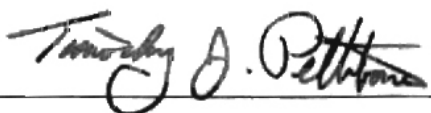
Thesis Approved:



Thesis Advisor







Dean of the Graduate College

PREFACE

The purpose of this research was to study the single-phase flow in structured packing using Computational Fluid Dynamics (CFD). This study will help in reducing the empiricism associated with the current packing manufacturing process. The work presented in this thesis is a step towards evaluating the reliability of CFD as a design tool, and will serve as a platform for future endeavors of CFD model development for structured packing. Effect of packing design parameters on the performance was studied, and flow patterns within a small section of two-sheet system (adjacent sheets) were analyzed.

I owe my gratitude to my advisor, Dr. Gary Foutch, for the opportunity to take part in this work. I learnt a lot from him, and I am thankful to him for the freedom I enjoyed while working on this project. I am also grateful to my thesis committee and co-advisors, Dr. Arland H. Johannes and Dr. Afshin J. Ghajar, for their invaluable guidance.

I am thankful to Dr. Joseph Smith for taking interest in this project. I really learnt a lot about CFD through the discussions we had. I really appreciate the assistance provided by Fractionation Research Inc., especially Dr. Kunesh and Dr. Tony Cai.

Most of all, I want to thank my parents for their support.

TABLE OF CONTENTS

Chapter	Page
1. INTRODUCTION.....	1
1.1 Distillation process.....	1
1.2 Structured packing.....	2
1.3 Rationale.....	4
1.4 Objectives.....	5
1.5 Thesis structure.....	6
2. LITERATURE REVIEW.....	7
Introduction.....	7
2.1 Structured packing: An overview.....	7
2.1.1 Evolution of structured packing.....	7
2.1.2 Geometrical features of structured packing.....	8
2.2 Modeling of structured packing.....	11
2.3 Computational Fluid Dynamics (CFD).....	17
2.3.1 History of CFD.....	17
2.3.2 Turbulence modeling.....	18
2.3.3 Terminologies associated with CFD.....	20
3. STRUCTURE OF CFX-5.5.1.....	25

Chapter	Page
3.1 Working of CFX-5.5.1	25
3.2 Mathematical details.....	28
4. RESULTS AND DISCUSSION.....	31
Introduction.....	31
4.1 Base case.....	33
4.1.1 Geometry.....	33
4.1.2 Mathematical models.....	35
4.1.3 Boundary conditions.....	37
4.1.4 Initial conditions.....	39
4.1.5 Meshing.....	39
4.1.6 Solver parameters.....	41
4.1.7 Convergence.....	42
4.1.8 Results for the base case.....	45
4.1.9 Comparison with experimental results.....	66
4.2 Effect of design parameters on the performance of packing.....	68
4.2.1 Effect of channel inclination angle.....	69
4.2.2 Effect of crimp angle.....	72
4.3 Effect of surface roughness.....	74
4.4 Effect of boundary condition.....	80
4.5 Large scale simulation.....	83
4.5.1 Model development.....	85

Chapter	Page
4.5.2 Results for large scale simulation.....	92
5. CONCLUSIONS AND RECOMMENDATIONS.....	95
5.1 Conclusions.....	95
5.2 Recommendations for future work.....	97
REFERENCES.....	99

LIST OF TABLES

Table		Page
4-1	Number of tetrahedral and prismatic elements.....	52
4-2	Effect of turbulence intensity on performance parameters.....	57
4-3	Effect of wall boundary condition on pressure drop.....	79
4-4	Variation of Splitting Factor with velocity.....	82

LIST OF FIGURES

Figure		Page
1-1	Graphical representation of structured packing block.....	3
1-2	Surface texture of MELLAPAK™ structured packing.....	4
2-1	Flow channel cross-section.....	8
2-2	Sheet geometry.....	9
4-1	Structured packing bed.....	31
4-2	Graphical representation of structured packing block.....	32
4-3	Channel orientation for structured packing sheets.....	32
4-4	geometry used for the CFD simulation of base case.....	34
4-5	Dimensions for channel cross-section.....	34
4-6	Flow paths downstream of the intersection zone.....	35
4-7	Volume mesh with inflated mesh elements.....	40
4-8	Mesh for the base case.....	41
4-9	Residual plot for mass and momentum equations.....	43
4-10	Residual plot for turbulence equations.....	44
4-11	Streamline plot	46
4-12	Vector plot for circled region in Figure 4-11.....	46

Figure	Page
4-13 Contour plot for tracer mass fraction at the center of the intersection zone.....	48
4-14 Expanded view of encircled portion in Figure 4-13.....	49
4-15 Contour plot for tracer mass fraction at Upper Channel outlet.....	49
4-16 Contour plot for tracer mass fraction at the center of the intersection zone (using 1 st order advection scheme).....	51
4-17 Contour plot for tracer mass fraction at the center of the intersection zone (using Second Order High Resolution Advection Scheme).....	51
4-18 Contour plot for tracer mass fraction at the center of the intersection zone (for Mesh I).....	54
4-19 Contour plot for tracer mass fraction at the center of the intersection zone (for Mesh II).....	54
4-20 Contour plot for tracer mass fraction at the center of the intersection zone (for Mesh III).....	54
4-21 Contour plot for tracer mass fraction at Upper Channel outlet (Mesh I).....	55
4-22 Contour plot for tracer mass fraction at Upper Channel outlet (Mesh II).....	55

Figure	Page
4-23 Contour plot for tracer mass fraction at Upper Channel outlet (Mesh III).....	55
4-24 Flow chart for Mesh Adaptation in CFX-5.....	59
4-25 Mesh for the 1 st Adaptation step.....	63
4-26 Mesh for the 2 nd Adaptation step.....	63
4-27 Contour plot for tracer mass fraction at the center of the intersection zone (1 st Adaptation step).....	65
4-28 Contour plot for tracer mass fraction at the center of the intersection zone (2 nd Adaptation step).....	65
4-29 Geometry similar to the one that has been Studied in the literature.....	67
4-30 Geometry similar to the one that is being used in this study.....	67
4-31 Structured packing sheet showing channel inclination angle.....	68
4-32 Channel cross section showing crimp angle.....	68
4-33 Location of channel inclination angle.....	69
4-34 Splitting Factor as a function of channel inclination angle for a crimp angle of 45°.....	70
4-35 Pressure drop as a function of channel inclination angle for a crimp angle of 45°.....	71

Figure	Page
4-36 Effect of channel inclination angle on Splitting Factor and pressure drop.....	71
4-37 Variation of Splitting Factor as a function of crimp angle for a channel inclination angle of 45°.....	73
4-38 Variation of pressure drop as a function of crimp angle for a channel inclination angle of 45°.....	73
4-39 Mesh generated to study the effect of surface roughness.....	76
4-40 Contour plot for tracer mass fraction at the center of the intersection zone.....	77
4-41 Mesh generated with 5 inflation layers	78
4-42 Mesh generated with 24 inflation layers.....	78
4-43 Contour plot for tracer mass fraction at the center of the intersection zone (For smooth wall with 24 inflation layers).....	79
4-44 Contour plot for tracer distribution at center of the intersection zone (velocity at Lower Channel Inlet= 1.5 m/s and Upper Channel Inlet = 2m/s).....	81
4-45 Contour plot for tracer distribution at center of the intersection zone (velocity at Lower Channel Inlet= 1 m/s and Upper Channel Inlet = 2m/s).....	81

Figure	Page
4-46 Streamline plot for flow entering at Lower Channel Inlet (velocity at Lower Channel Inlet= 1 m/s and Upper Channel Inlet = 2m/s).....	82
4-47 Two-sheet geometry with thirty channels	83
4-48 Two-sheet geometry with 12 channels.....	84
4-49 Sheet dimensions for the geometry show in Figure 4-48.....	85
4-50 Channel cross section for Figure 4-48.....	85
4-51 Inlet and outlet B.C. for two-sheet geometry.....	86
4-52 Streamline plot for UI 1.....	88
4-53 Streamline plot for UI 2.....	88
4-54 Streamline plot for UI 3.....	88
4-55 Streamline plot for UI 4.....	88
4-56 Streamline plot for LI 1.....	89
4-57 Streamline plot for LI 2.....	89
4-58 Streamline plot for LI 3.....	89
4-59 Streamline plot for LI 4.....	89
4-60 Tracer mass fraction distribution with tracer introduced at UI 1.....	92
4-61 Measure tracer distribution in two-sheet system for Montz packing.....	92
4-62 Tracer mass fraction distribution with tracer introduced at LI 1.....	93

Figure		Page
4-63	Tracer mass fraction distribution with tracer introduced at UI 4.....	93
4-64	Flow pattern for the flow entering at LI 4.....	94

NOMENCLATURE

Symbols

D_{ϕ}	Kinematic diffusivity of additional variable, m^2/s
g	Gravitational acceleration, m/s^2
k	Turbulence kinetic energy per unit mass, m^2/s^2
p	Pressure, N/m^2
S_{ϕ}	Source term for additional variable, $1/s$
Sc	Schmidt Number, dimensionless
t	Time, s
U	Mean velocity, m/s
u'	Turbulence fluctuation velocity, m/s

Greek Letters

ρ	Density, Kg/m^3
ϵ	Turbulence dissipation rate m^2/s^3
μ	Dynamic viscosity, $N-s/m^2$

μ_t	Eddy viscosity, N-s/m ²
μ_{eff}	Effective viscosity, N-s/m ²
Φ	Additional variable, Kg/Kg

CHAPTER 1

INTRODUCTION

1.1 Distillation process

The separation of a homogeneous liquid mixture into its individual components is an important step in many industrial processes. Of the various processes that might be used to achieve the separation, distillation is the most widely used method. Distillation uses a very simple separation principle: an intimate contact is created between the starting mixture and a second phase in order to enhance effective mass transfer between. The thermodynamic conditions are chosen such that the constituent to be separated from the mixture transfers to the second phase. The phases are subsequently separated into two single phases with different compositions (Stichlmair et al., 1998). As per the Research and Development Portfolio, Published by US Department of Energy in April 1999, separation processes represent up to 70% of capital and operating costs and accounts for nearly 45% of the energy used in the chemical process industries. Distillation contributes a major part of this energy requirement, estimated at US\$524 billion per annum (Porter, 1995). Therefore, any improvement in the distillation process will result in significant monetary and energy savings.

Separation within a distillation column is achieved through either tray or packed type contacting devices. In tray type columns, the gas flows vertically upward through

small perforations in horizontal trays, while liquid flows across the tray. In packed columns, a high interfacial area for mass transfer between gas and liquid is provided by filling the column with a bed of solid materials with high porosity and large volumetric area. The liquid trickles downward in the form of thin films, small rivulets and even small droplets. Trays are used in large diameter columns and can be operated efficiently at very low liquid loads. However, relatively high-pressure drop and high liquid hold up are the disadvantages associated with the use of tray columns. Packed columns are used almost exclusively in small diameter (e.g. smaller than 0.7 m) towers. The small pressure drop in packed column relative to the tray column is a big advantage. Also, the danger of decomposition of thermally unstable substances is also less in packed columns because liquid holdup is very small (Stichlmair et al., 1998).

1.2 Structured packing

Packings can be classified as random and structured. Random packing is dumped in the column whereas structured packing has regular arrangement. The random distribution leads to liquid maldistribution, which adversely affects the mass transfer efficiency. This resulted in the development of structured packing. In comparison to random packing, structured packing permits higher mass transfer efficiency at lower power consumption, thus achieving an economy in column scale and operating costs. In structured packing, corrugated sheets are assembled parallel in vertical direction with alternate inclination of corrugation of neighboring sheets (Stichlmair et al., 1998).

The liquid flows as a film on the packing surface and gas flows through the channels formed between the neighboring sheets. These corrugated sheets are grouped together in a block. An example of a structured packing block is presented in Figure 1-1.

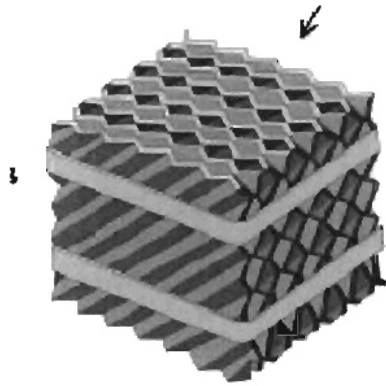


Fig 1-1 A graphical representation of a structured packing block ⁽¹⁶⁾

The blocks of packing are installed as layers that fill the cross sectional area of the column. These layers are stacked, atop another, to give the required packed height. Adjacent layers are rotated 90° to enhance lateral mixing of liquid and gas. This arrangement results in an ordered network of flow channels. Structured packing is treated mechanically and/or chemically in order to improve the liquid wetting characteristics. The surface treatment can affect both the surface area available for mass transfer and the liquid film turbulence. Embossing and creating fluted surface are some examples of surface treatment.

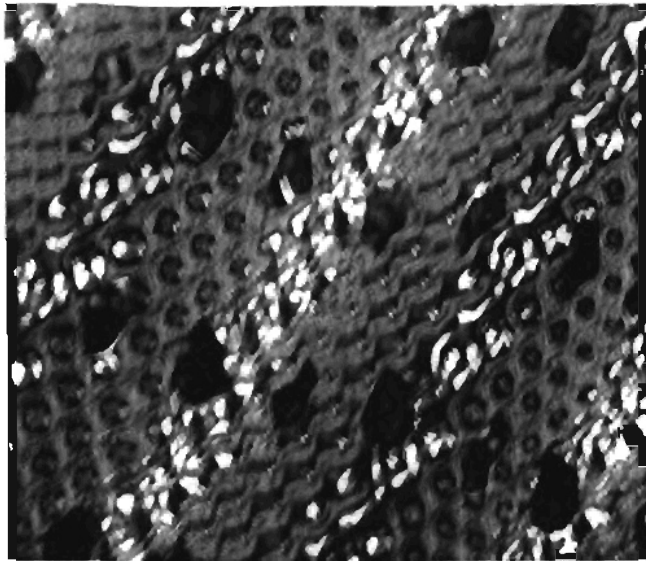


Fig 1-2 Surface texture and perforations of MELLAPAK™ structured packing

1.3 Rationale

Almost all the traditional design equations developed to describe fluid flow and mass transfer in structured packing involve one or more empirical constants. These equations are applicable in the range of the experimental conditions under which the constants were determined and are specific to a particular type of packing. Empiricism restricts the use of these equations and limits their usefulness in designing new packing. The work proposed in this thesis started with an effort to model the flow distribution within an entire distillation column Computational Fluid Dynamics (CFD). During the course of the work, it was realized that computationally it is not feasible to model the micro scale/local phenomena (for example, mixing occurring at an intersection of crossing channels in structured packing) in detail. Therefore, these local phenomena need

to be approximated by proper models for which detailed understanding of the local phenomena will be required. This process is analogous to large eddy simulations in turbulence, where large scale eddies are solved directly without any approximations and small scale eddies are approximated using turbulence models.

1.4 Objectives

The aims of this thesis are to use the approach of Computational Fluid Dynamics to:

- 1) Provide an understanding of the flow physics in structured packing on micro/local scale, which can serve as a platform for future endeavors of CFD model development for structured packing.
- 2) Study the effect of structured packing design parameters (channel inclination angle and crimp angle) on performance (pressure drop and mixing characteristics).
- 3) Study the flow pattern in a section of adjacent corrugated sheets with alternate corrugation inclination.

1.5 Thesis Structure

- 1) A brief literature review, giving the evolution of structured packing, and the previous work that has been done to model the structured packing, will be discussed in second chapter. Also, a brief overview of CFD will be given.
- 2) The procedures and methods used while working with the CFD code used for this study (CFX-5.5.1) will be discussed in Chapter 3.
- 3) CFD model development and results will be presented in Chapter 4.
- 4) Final discussion and conclusions will be addressed in Chapter 5.

CHAPTER 2

LITERATURE REVIEW

Introduction

The literature review addresses the topics of structured packing and Computational Fluid Dynamics (CFD) in two sections. In the structured packing section, first a brief overview of the evolution of structured packing design will be given. Secondly, previous work in the area of modeling fluid flow and mass transfer in structured packing will be discussed. In the CFD section, present state of the art in CFD modeling will be presented.

2.1 Structured packing: An overview

2.1.1 Evolution of structured packing

Although structured packings have been around as early as the 1940's, the earlier models such as Panpak[®] never became popular. One reason for this unpopularity could be the fact that this was before the time when the detrimental effect of liquid maldistribution on structured packing was known. The second generation of structured packing began in the late fifties with high efficiency wire-mesh packings like the Goodloe[®], Hyperfil[®], and Koch-Sulzer. Extensive experimentation, led by Sulzer, provided insight into

maldistribution, and the knowledge was applied for successful scale up. By early 1970's, use of structured packing increased significantly into vacuum distillation, where their low pressure drop per theoretical stage is a major advantage. Their high cost, high sensitivity to solid and low capacity hindered application of the wire-mesh packing outside vacuum distillation. The corrugated-sheet structured packing, first introduced by Sulzer in the late 1970's, started a new generation of structured packing. With a high capacity, lower cost, and lower sensitivity to solids, while still retaining high efficiency, this corrugated sheet packing became competitive with conventional internals. The 1980's saw an accelerated rise in popularity of structured packing, becoming one of the most popular column internals in use today. Presently, the popular corrugated sheet structured packings are Mellapak[®], Flexipac[®], Gempak[®], Montz B1[®], MAX-PAC[®], Montz BSH[®], and Flexeramic[®] (Kister, 1992).

2.1.2 Geometrical features of corrugated structured packing

a) Crimp geometry/flow channel cross-section geometry

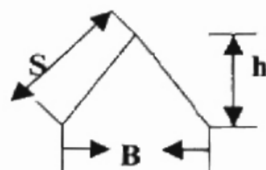


Fig 2-1 Flow channel cross-section

The relative ratio of B to h, S to h, and the crimp angle (angle between side S and base B), defines the geometry of the flow channel and of the vapor liquid contact zone. In different packing families, crimp angle varies from 28° to 45° and B to h ratios range from 2:1 to 4:1 (Kister, 1992).

b) Sheet geometry

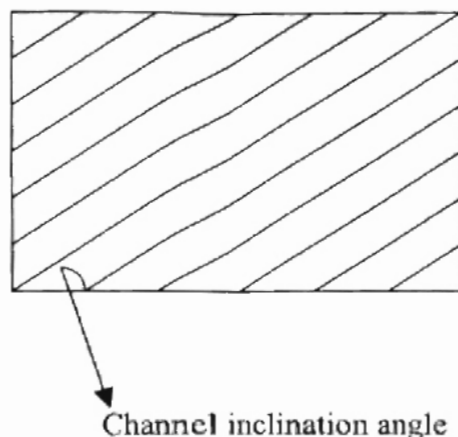


Fig 2-2 Sheet geometry

The inclination angle of the channels may range from 15° to 60° ; 45° is most popular. Gaiser and Kottke (1989) showed the effect of channel inclination angle on flow pattern and hence the local heat and mass transfer. They found that at high inclination angle and a small B: h ratio, the major part of the flow following the valley gets reflected at the wall and returns along the valley of the neighboring sheet. Whereas, at low inclination angles and a large B: h ratio, a greater part of the flow is in the main flow direction, between the contact points of adjacent sheets. Olujić et al. (2000) presented an experimental study revealing the effect of packing geometry and corrugation angle on

mass transfer and hydraulic performance for Montz packing. With increasing corrugation angle (also called as channel inclination angle), the pressure drop decreases sharply. The accompanying increase in capacity and decrease in mass transfer efficiency are an order of magnitude less pronounced, indicating that a significant amount of pressure drop is not directly involved with the mass transfer process. Increasing the ratio of the “useful” to “useless” (the gas-gas interaction and direction change) pressure drop is the key to further improvement of the performance of corrugated sheet structured packing.

c) Surface texture

Most structured packings have a roughened or enhanced surface that assists the lateral spreading of liquid, promotes film turbulence, and enhances the area available for mass transfer. Laboratory measurements of absorption rates showed that both mass transfer efficiency and wetted area are enhanced by texturing metal surfaces. Texturing techniques include grooving, lancing, shallow embossing, and deep embossing. Surfaces of most structured packings contain perforations, which serve as communication channels between the upper and lower surface of each sheet. Usually, the perforations are of circular shape (Kister, 1992).

2.2 Modeling of structured packing

With the increasing use of structured packing, various models are proposed to predict their performance. Most of the models are based on some empirical constants. This empiricism makes the models applicable to only the existing designs of structured packing.

Zuiderweg et al. (1993) proposed a zone/stage model to predict the influence of initial liquid distribution on the liquid flow distribution inside the column and the overall efficiency of the packed column. The model can be applied to both random and structured packing. But, the model requires two packing characteristics as input: a liquid spreading coefficient and an "ideal" or "basic" HETP. These values need to be determined experimentally.

Stoter et al. (1993) proposed a mathematical model, based on first principles, for the calculation of gas flow distribution in channels formed between the tightly packed corrugated sheets. The model neatly explains the physics of fluid flow in crisscrossing network of structured packing. The model uses a discrete cell approach, based on average mass, momentum, and energy balance equations for each of numerous crossings of gas flow channels. Characteristic friction factors for gas inlet, bulk zone, and wall zone are required model parameters. These model parameters need to be obtained from pressure drop measurements for each type and size of structured packing. The model assumes complete wetting of the packing surface and thus the liquid holdup is expressed as a function of an average liquid film thickness and packing surface area.

Shetty and Cerro (1997) developed correlations for estimating design parameters (liquid hold up, interfacial area, and mass-transfer coefficient) in ordered packing materials based on fluid mechanics and mass transfer without any adjustable parameters. The effect of the size of structured packing as well as liquid properties on these parameters was explored. Mass-transfer coefficients for the liquid phase were estimated using a penetration theory model. These parameters were used to predict height of a transfer unit (HTU) and height equivalent to a theoretical plate (HETP) for typical commercial packing materials and compared with existing experimental data.

A mechanistically based model was developed by Rocha et al. (1993) to predict liquid hold up, pressure drop, and flooding in columns containing structured packing. The correlations were based on the approach of considering the flow channels within the packing as a series of wetted wall columns with a geometry that depends on the angle and size of the packing. The model takes into account the texturing of the packing surface as well as the wettability of the surface material when in contact with various types of liquids. The model was able to predict the pressure drop above, as well as below, the load point.

Iliuta and Larachi (2001) developed an implicit one-dimensional two-zone, two-fluid mechanistic model for the prediction of the irrigated two-phase pressure drop, total liquid holdup, and the packing fractional wetted area in gas liquid columns containing structured packing. The model is applicable in the preloading zone. The two-phase flow topography was approximated using two inclined and interconnected slits. Out of the two

slits, the dry slit is solely fed by gas and a gas-liquid slit fed by liquid and remaining gas. Their model requires no adjustable parameter.

Spiegel et al. (1996) proposed a method to predict the heat transfer coefficient for structured packing, based on the experimental study with air/water and air/oil system for Mellapak™ 250.Y, 250.X, and 125.X.

Carmen Rey et al. (1998) investigated the influence of natural convection (for low velocities) on mass transfer coefficient for structured packing. This is a unique study, because all other literature studies are related to high Reynolds number. Low velocities are used in applications like bioreactors. A simple model was formulated, which describes natural convection mass transfer in structured packing by correlations obtained for inclined surfaces.

Hanley et al. (1994) proposed a new approach of percolation theory to predict the two-phase pressure drop in a packed column. The approach is based on the concept of conductor/insulator transition in electrical lattice. The flow passage, making up the void spaces of the packing, are taken to be “conducting” when they are open to vapor flow and “insulating” when they are choked off by the liquid (i.e. localized flooding). The same approach was used to develop correlations for mass-transfer coefficients, mass-transfer area, the HETP, and dynamic liquid holdup (Hanley et al., 1994).

Edwards et al (1999) proposed a concept of depth of penetration of maldistribution in columns packed with structured packing and a method to estimate the depth. Vapor flow is modeled as flow through an isotropic porous media (modeled by the

Ergun equation). For liquid flow calculations, an approximate solution for a point source in an infinite domain was used. The correlations developed do not take into account the effect of liquid vapor interaction.

Design, scale-up, and performance analysis procedures for packed columns have been traditionally based on macroscopic mass balances. Successful design and scale-up of packed columns require a model that captures the basic transport phenomena on the scale of packing and not on the scale of the equipment. CFD models can be used to predict the overall separation efficiency based on local conditions. The CFD models, however, require the specification of number of closure models to capture the information lost during the averaging process. These closure models should provide the interaction of transport processes between the phases on a scale smaller than the averaging scale (Nandakumar et al., 2000).

Hodson et al. (1997) studied the single-phase fluid flow in structured packing using CFD. This was the first effort, to the best knowledge of the author, to use CFD to model the processes occurring within structured packing. Modeling efforts in the past are mostly based on fitting experimental data to semi-empirical expressions i.e. modeling on micro- scale. The proposed CFD model takes a different approach of modeling the processes occurring on micro-scale within the channels of structured packing. The model focuses on the intersections or junctions between the channels in neighboring sheets of packing. The solution proceeds in a stepwise manner by performing successive simulations on one junction: Outlets from one junction act as inlets to next. A heat transfer model was used to study the effect of packing geometry on heat transfer (which

is analogous to mass transfer). Based on the heat transfer results, a new packing design with slots and tabs punched out of the apex of the channels was proposed.

Krishna et al. (2001) studied the radial, and axial, liquid-phase dispersion within the catalytically packed crisscrossing sandwich structure of KATAPAK-S using CFD. The crisscrossing structure of the KATAPAK-S was modeled as a set of intersecting, connecting, triangular tubes. Ergun equation was used to model the catalytic packing inside the crisscrossing. Residence time distribution simulation was conducted to calculate the liquid radial dispersion coefficient.

Gulijk (1998) used the CFD approach, similar to Krishna et al. (2001) to calculate the transversal dispersion coefficient in a structured packed bed. The transversal dispersion coefficient was found to be 40 times that of fixed bed value.

Recently Petre et al. (2003) proposed a predictive combined mesoscale-microscale methodology using CFD to apprehend the aerodynamic phenomena occurring at the macroscale in structured packing containing columns. The postulate rests on identifying recurrent dissipation patterns, called as Representative Elementary Unit, REU, constituting the geometry of the structured packing. CFD microscale simulations were carried out to determine different REU loss coefficients. Appropriate REU-bed mapping equations were developed to allow clustering of the REU loss coefficients into a global bed-scale loss coefficient for estimating the total pressure drop. The simulation results were in accordance with the experimental results published for different packings. A CFD-aided development methodology was also proposed for Montz B1-250 structured packing recasting the detailed information into compact macroscopic numerical

coefficient for the total loss coefficient similar to Ergun equation. The laminar, turbulent, and curvature parameters appearing in these correlations were expressed as a function of the corrugation angle.

There have been some efforts to use CFD to study fluid flow through fixed bed (random packing)

Parsons et al. (1992) analyzed the single-phase flow patterns in random packing bed using CFD. Resistance to fluid flow was modeled using the Ergun equation.

Mohammed et al. (2002) presented the results of first large scale experimental effort undertaken to collect experimental evidence necessary for appropriate validation of a results from a commercial CFD package, FLUENT 5. The authors used FLUENT 5 to predict the extent of gas maldistribution introduced by geometry of column internals. A quarter of the liquid distributor was simulated assuming symmetry.

Nandakumar et al. (2000) proposed a CFD- based approach of volume-averaged equations for velocity and concentration fields to simulate the hydrodynamics and mass-transfer processes in a randomly packed distillation column.

Logtenberg and Dixon (1998) studied the fluid flow and heat transfer in a fixed bed of tube to particle ratio 2.86 using a commercial finite element code, ANSYS/FLOTRAN. In another study, Jiang et al. (2001) used CFDLIB code, developed by Los Alamos Laboratory, to model the multiphase flow distribution in catalytic packed bed reactors.

2.3 Computational Fluid Dynamics (CFD)

Computational fluid Dynamics (CFD) is a computer-based tool for simulating the behavior of systems involving fluid flow, heat transfer, mass transfer, and other related physical processes. It works by solving the equations of fluid flow over a region of interest, with specified conditions on the boundary of that region.

2.3.1 History of CFD

Computers have been used to solve fluid flow problems for many years. Numerous programs have been written to solve either specific problems, or specific classes of problem. From the mid-1970's, the complex mathematics required to generalize the algorithms began to be understood, and general-purpose CFD solvers were developed. These began to appear in the early 1980's and required what were then powerful computers, as well as in-depth knowledge of fluid dynamics, and large amount of time to set up simulations. Consequently, CFD was a tool used almost exclusively in research.

Recent advances in computational power, together with powerful graphics and interactive 3-D manipulation of models mean that the process of creating CFD model and analyzing the results is much less labor-intensive, reducing the time and therefore the cost. Advanced solvers contain algorithms, which enable robust solution of the flow field

in a reasonable time. As a result of these factors, CFD is now an established industrial design tool, helping to reduce design timescales and improving processes throughout the engineering world. CFD provides a cost-effective and accurate alternative to scale model testing, with variations on the simulations being performed quickly, offering obvious advantages.

2.3.2 Turbulence Modeling

Commercially-available general-purpose CFD codes often ignore transition region (from laminar to turbulent flow) and classify flows as either laminar or fully turbulent. A crucial difference between the visualization of laminar and turbulent flows is the appearance of eddying motions of wide range of length scales in turbulent flows. A typical flow domain of 0.1 by 0.1 m with a high Reynolds number turbulent flow might contain eddies down to 10 to 100 μm size. We would need computing meshes of 10^9 to 10^{12} points to be able to describe processes at all length scales. The fastest events take place with a frequency of about 100 μs (Versteeg et al., 1995). Speziale (1991) states that the direct simulation of a turbulent pipe flow at a Reynolds number of 500000 requires a computer which is 10 million times faster than current generation CRAY supercomputer. With present day computing power it has only recently started to become possible to track the dynamics of eddies in very simple flows at transitional Reynolds number. The computing requirements for the direct solution (DNS) of the time dependent Navier-Stokes equations of fully developed turbulent flows at high Reynolds number are truly phenomenal and must await major developments in computer (Versteeg et al., 1995). In

most of the engineering applications it is not required to resolve each and every eddy in the flow. Therefore the Navier-Stokes equation for turbulent flow is time averaged as expressed by Equation 2-1.

$$\rho \frac{D\bar{U}}{Dt} + \rho \frac{\partial}{\partial x_j} (\overline{u'_i u'_j}) = \rho g - \nabla \bar{p} + \mu \nabla^2 \bar{U} \quad (2-1)$$

The time-averaged Navier-Stokes equation resulted in six additional unknowns called Reynolds stresses. It is the main task of turbulence modeling to develop computational procedures of sufficient accuracy and generality to predict the Reynolds stresses. Turbulence models listed in literature are:

- 1) The Zero equation model: Mixing length model
- 2) Two-equation model: k- ϵ model
- 3) Reynolds stress equation model
- 4) Algebraic stress model

The mixing length and k- ϵ models are most used and validated turbulence models for engineering applications. They are based on the assumption that there exists an analogy between the action of viscous stresses and Reynolds stresses on the mean flow. The Zero equation model is easy to implement and cheap in terms of computing resources, but the model is incapable of describing flows with separation and recirculation. The k- ϵ model is more sophisticated than the zero equation model. But, the k- ϵ model fails to give

correct results in certain cases; for example, some unconfined flows, flows with large extra strains, rotating flows, fully developed flows in non-circular ducts (Versteeg et al., 1995).

2.3.3 Terminologies associated with CFD

a) Discretization:

Analytical solutions to the Navier-Stokes equation exist for only the simplest of flows under ideal conditions. For real flows the governing equations need to be solved numerically. Discretization refers to the numerical approach of replacing the governing equations by algebraic approximations, which may be solved using a numerical method.

b) Mesh/Grid generation

Grid generation can be defined as the sub-division of the computational domain into a number of smaller, non-overlapping sub-domains.

c) Structured mesh

The grid is laid out in a regular repeating pattern. These types of grids utilize quadrilateral elements in 2D and hexahedral elements in 3D (html link ^[39])

d) Unstructured mesh

Unstructured grid methods utilize an arbitrary collection of elements to fill the domain. These types of grids typically utilize triangles in 2D and tetrahedra in 3D (html link ^[39])

e) Finite volume solution technique (Versteeg et al., 1995)

The numerical algorithm of finite volume scheme consists of following steps:

- Formal integration of the governing equations of fluid flow over all the control volumes of the solution domain
- Discretization involves the substitution of a variety of finite-difference type approximations for the terms in the integrated equations representing flow processes such as convection and diffusion. This converts the integral equations into a system of algebraic equations.
- Solution of the algebraic equations by iterative method

f) Finite element technique

Finite element methods use simple piecewise functions (e.g. linear or quadratic) valid on elements to describe the local variations of unknown flow variables Φ .

g) Advection scheme

Advection scheme is used for the discretization of the convective terms in the governing equation

h) Convergence: ([html link](#) ^[40])

1) Grid convergence

Grid convergence indicates that as the grid spacing is reduced, the computed simulation results approach the continuum result. Here "grid spacing" can refer to both spatial spacing, as well as, time step for the case of unsteady, time-accurate simulations.

2) Iterative convergence

Iterative convergence indicates that as the discrete equations are iterated, the computed simulation results approach a fixed value. The criteria to determine the iterative convergence include:

i) *Residuals*

The residuals of the equations are the change in the equations over iteration. These are usually scaled or normalized. One usually looks for the residuals to reach a certain level as an indication of iterative convergence. For a time-marching, steady-state strategy, this involves examining whether the residual has been reduced a certain number (usually 3-4) of orders of magnitude.

ii) *Results*

The CFD simulation has the objective of determining some quantity such as lift, drag, recovery, etc. One can track the values of such engineering quantities with respect to iteration and define iterative convergence when these quantities converge. The

convergence criteria are usually defined by acceptable error in these values. It is often the case that certain quantities may reach convergence at a different rate than other quantities. One can check that a monitored flow value (such as thrust, drag, or boundary layer profile) has remained unchanged with respect to the number of iterations.

iii) *Time-Accurate Simulations*

For a time-marching, time-accurate strategy, this involves examining whether the final time has been reached with proper convergence at each time step.

iv) *Space-Marching Simulation*

For a space-marching strategy, this involves examining whether the end of the marching segment has been reached with proper convergence at each marching step.

i) *Validation*

Validation is the process of determining the degree to which a model is an accurate representation of the real world from the perspective of the intended uses of the model (html link ^[40]).

j) *Verification*

Verification is the process of determining that a model implementation accurately represents the developer's conceptual description of the model and the solution to the model (html link ^[40]).

k) Numerical diffusion

Numerical diffusion is usually exhibited by difference equations where the advection term has been approximated using an odd-ordered advection scheme, for example, Upwind Differencing Scheme, which is first order accurate. This causes the distributions of the transported properties to become smeared. The resulting error has a diffusion-like appearance (CFX-5.5.1 user manual)

l) Numerical dispersion

Numerical dispersion is usually exhibited by discretized equations whose advection terms has been approximated using schemes that are even order accurate, for e.g. central difference scheme, which is second order accurate. Dispersion results in oscillations or wiggles in the solution particularly where there are steep flow gradients (CFX-5.5.1 user manual)

CHAPTER 3

STRUCTURE OF CFX-5.5.1

3.1 Working of CFX-5.5.1

In the present study, the CFD code used is CFX5.5.1. CFX-5.5.1 is the latest upgrade in CFX-5 series (CFX- 5.6 is scheduled for release in May). CFX-5 is a general purpose CFD code (marketed by ANSYS), combining an advanced solver with powerful pre and post processing capabilities. This section is intended to briefly describe the working of CFX-5. For detailed reading, CFX-5.5.1 user manual is recommended.

The process of performing single CFD simulation is split into three components:



Pre-processor

The pre-processor is the component used to create the input for the solver. Pre-processing involves:

- a) Defining the geometry of the region of interest
- b) Selecting the physical models which are to be included in the simulation

- c) Specifying the properties of the fluid
- d) Specifying the boundary conditions
- e) Creating a mesh of control volumes

In CFX-5.5.1, CFX-Build acts as pre-processor. In addition to its own geometry tools, CFX-Build can import geometries from other major CAD packages. CFX-Build also provides high-level automatic mesh generation tools, significantly reducing mesh generation times.

Solver

The solver is the component which solves the CFD problem, producing the required results. The process can be described as follows:

- a) The partial differential equations are integrated over all the control volumes in the region of interest. This is equivalent to applying a basic conservation law (e.g. for mass or momentum) to each control volume.
- b) These integral equations are converted to a system of algebraic equations by generating a set of approximations for the terms in the integral equations.
- c) The algebraic equations are solved iteratively.

An iterative approach is required because of the non-linear nature of the equations and as the solution approaches the exact solution it is said to be converged. For each iteration an error, or residual, is reported as a measure of the overall conservation of the flow

properties. How close the final/converged solution is to the exact solution depends on a number of factors, including the size and shape of the control volumes and the size of the final residuals. Complex physical processes, such as combustion and turbulence are often modeled using empirical relationships, and the approximations inherent in these models also contribute to differences between the CFD solution and the real flow. The solution process requires no user interaction. The solver produces a result file, which is then passed on to the post-processor. In CFX-5.5.1, the solver process is managed by CFX-Solver Manager.

Post-processor

The post-processor is the component used to analyze and present the results. Post-processing involves anything from obtaining point values to complex animated sequences.

Examples of some important features of post-processors are:

- a) Visualization of the geometry and control volumes
- b) Vector plots showing the direction and magnitude of the flow
- c) Visualization of the variation of scalar variables (such as temperature) through the domain
- d) Quantitative numerical calculations
- e) Animation

f) Charts showing graphical plots of variables

g) Hardcopy output

In CFX-5.5.1, post-processing is achieved through CFX-Post.

3.2 Mathematical Details

There are number of different solution methods which are used in CFD codes. The most common, and the one on which CFX-5 is based, is known as the finite volume technique (Refer section 2.3.3 for details). The advection scheme implemented in CFX-5.5.1 can be expressed in the form:

$$\phi_{ip} = \phi_{up} + \beta \nabla \phi \cdot \Delta r \quad (3-1)$$

Where ϕ_{up} is the value of the upwind node, $\nabla \phi$ is the gradient of ϕ and r is the vector from the upwind node to the ip . Particular choices for β give rise to different schemes.

CFX-5 uses a single cell, unstaggered, and collocated grid to overcome the decoupling of the pressure and/or velocity.

Coupled Solver

One of the strength of CFX-5 is its coupled solver. Segregated solvers employ a solution strategy where the momentum equations are first solved, using a guessed pressure, and an equation for a pressure correction is obtained. Because of the guess-and-

correct nature of the linear systems, a large number of iterations are typically required in addition to the need for judiciously selecting relaxation parameters for these variables. CFX-5 uses a coupled solver, which solves the hydrodynamic equations (for u , v , w , p) as a single system. The solution approach uses a fully implicit discretization of the equations at any given time step. For steady state problems the time-step behaves like an acceleration factor, to guide the approximate solutions in a physically based manner to a steady state solution. This reduces the number of iterations required for convergence to a steady state, or to calculate the solution for each time step in a time dependent analysis.

The solution procedure in general follows the following two steps:

- 1) The non-linear equations are linearized and assembled into the solution matrix.
- 2) The linear equations are solved using an Algebraic Multigrid method. (The convergence behavior of many matrix inversion techniques can be greatly enhanced by the use of technique called multigrid. The multigrid process involves carrying out early iterations on a fine mesh and later iterations on progressively coarser virtual ones. The results are then transferred back from the coarsest mesh to the original fine mesh. CFX-5 uses a particular implementation of Algebraic Multigrid called Additive Correction)

Turbulence models

Turbulence models offered by CFX-5.5.1 cover a wide range of engineering applications.

- a) The Zero Equation model

- b) Standard k - ϵ model
- c) RNG k - ϵ model
- d) Standard k - ω model
- e) Baseline (BSL) zonal k - ω model
- f) SST zonal k - ω based model
- g) Reynolds-Stress model
 - a) Launder, Reece, and Rodi Isotropization of Production model (LRR-IP)
 - b) Launder, Reece, and Rodi Quasi-Isotropic model (LRR-QI)
 - c) Speziale, Sarkar, Gatski model (SSG)

CHAPTER 4

RESULTS AND DISCUSSION

Introduction

A packed bed of structured packing consists of blocks of structured packing one atop another as shown in Figure 4-1.

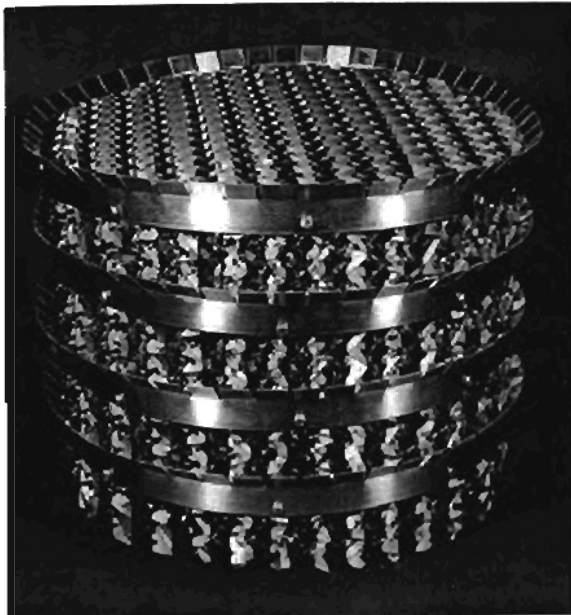


Figure 4-1 Structured packing bed (Krishna et al., 2001)

Each block is made of structured packing sheets placed adjacent to each other in such a way that two adjacent sheets have different channel orientation as shown in Figure 4-2 and 4-3.

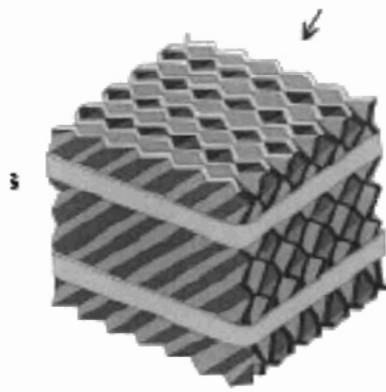


Fig 4-2 A graphical representation of a structured packing block (Krishna et al., 2001)

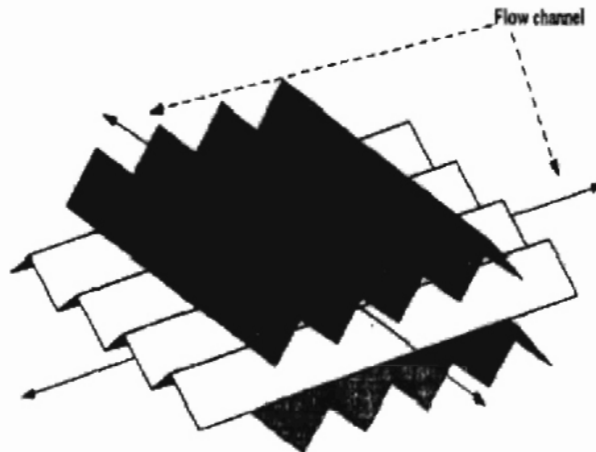


Fig 4-3 Channel orientation for structured packing sheets

The triangular channels of adjacent sheets intersect each other at an angle decided by the channel inclination angle. Two adjacent sheets in a structured packing block can be seen as an ordered network formed by repeating an elementary unit cell shown in Figure 4-4. The elementary unit consists of an intersection zone formed by the channels of adjacent sheets.

4.1 Base case

4.1.1 Geometry

For the base case, a channel inclination angle of 45° is considered i.e. the two flow channels intersect at an angle of 90° . The flows in the two channels interact with each other at the intersection zone. The geometry for the base case, used in the CFD simulation, is shown in Figure 4-4. The channel cross-section dimensions are shown in Figure 4-5. Downstream of the intersection zone, the flow from each channel has three possible paths to follow. The flow paths are shown in Figure 4-6. In Figure 4-6, the flow is entering at Upper Channel inlet. The three possible flow paths are:

1. The flow will follow the Upper Channel (Path 1)
2. The flow will follow the Lower Channel (Path 2)
3. The flow will get split at the intersection with a fraction of the flow following the Upper Channel and remaining flow entering the Lower Channel.

In past, visualization experiments have been conducted to study the flow profile in intersecting square ducts/ channels (Umeda et al., 1994; Zhang et al., 1993). It was observed that the flow followed the third possibility mentioned above. For the base case geometry, if the flow gets split at the intersection, the flow entering the Lower Channel is expected to show the characteristics as that of the flow in a 90° bend (since the two channels intersect at 90°). Therefore, it is expected that the flow entering the Lower Channel will result in a recirculation zone due to flow separation. For CFD simulation, the location of the outlet should be such that vortices are far enough from the outlet so that their influence on flow solution is minimal. For the base case, a trial and error analysis showed that a distance of 36 mm (equal to the length of the channel base),

downstream of the intersection zone, is sufficient to satisfy the above mentioned criterion. The total length of each channel is 108 mm (36*3).

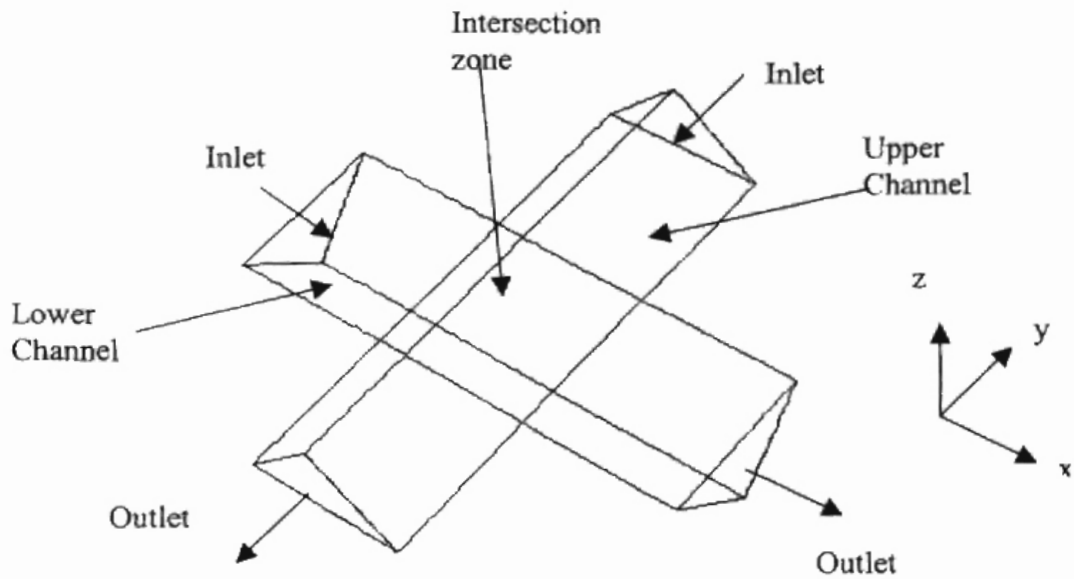


Fig 4-4 Geometry used for the CFD simulation of base case

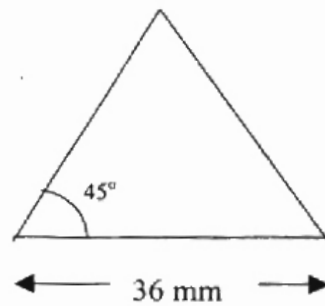


Fig 4-5 Dimensions for channel cross-section

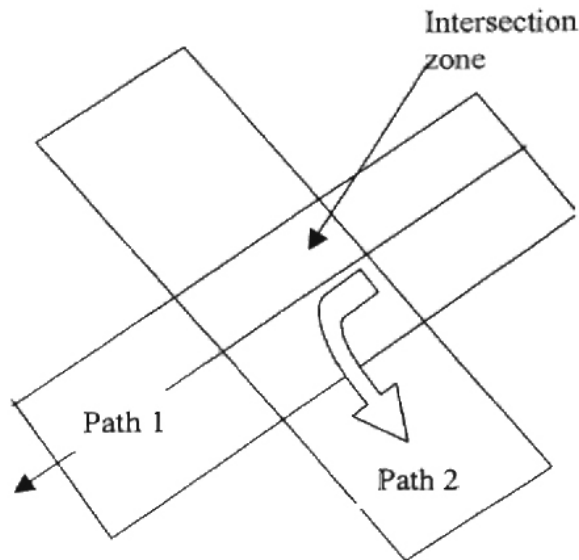


Fig 4-6 Flow paths downstream of the intersection zone (Top view of Figure 4-4)

4.1.2 Mathematical models

Air as an ideal gas is modeled in the flow domain shown in Figure 4-4 with the domain operating pressure set to $1.013 \times 10^5 \text{ N/m}^2$. The fluid domain is assumed to be isothermal with a constant temperature of 298 K. Since the Reynolds Number, for the flow conditions considered in the simulation, is less than 10,000, the two-equation RNG k- ϵ turbulence model is used. The RNG k- ϵ turbulence model is based on the renormalization group analysis of the Navier-Stokes equations. The transport equations for turbulence generation and dissipation are the same as those for the standard k- ϵ model, only the model constants differ.

The transport equation for turbulence dissipation is:

$$\frac{\partial \rho \epsilon}{\partial t} + \nabla \cdot (\rho U \epsilon) - \nabla \cdot \left(\frac{\mu_{eff}}{\sigma_{\epsilon RNG}} \nabla \epsilon \right) = \frac{\epsilon}{k} (C_{\epsilon 1 RNG} P_k - C_{\epsilon 2 RNG} \rho \epsilon) \quad (4-1)$$

The transport equation for turbulence kinetic energy is:

$$\frac{\partial \rho k}{\partial t} + \nabla \cdot (\rho U k) - \nabla \cdot \left(\frac{\mu_t}{\sigma_k} \nabla k \right) = P_k - \rho \varepsilon \quad (4-2)$$

P_k is the shear production due to turbulence, which for incompressible flows is given as:

$$P_k = \mu_t \nabla U \cdot (\nabla U + \nabla U^T) - \frac{2}{3} \nabla \cdot U (\mu_t \nabla \cdot U + \rho k) \quad (4-3)$$

σ_k , $C_{\varepsilon 1RNG}$, $C_{\varepsilon 2RNG}$ are constants, whose value is given as

$$\sigma_k = 1$$

$$C_{\varepsilon 2RNG} = 1.68$$

$$C_{\varepsilon 1RNG} = 1.42 - f_\eta$$

$$f_\eta = \frac{\eta(1 - \frac{\eta}{4.38})}{(1 + \beta_{RNG} \eta^3)}$$

$$\eta = \sqrt{\frac{P_k}{\rho C_{\mu RNG} \varepsilon}}$$

$$C_{\mu RNG} = 0.085; \beta_{RNG} = 0.012$$

To study the mixing of the flow at the intersection zone, a tracer simulation was carried out by solving the scalar equation for an additional variable. The additional variable considered in this study is the mass fraction of the tracer. The additional variable equation is given by Equation 4-4.

$$\frac{\partial \Phi}{\partial t} + \nabla \cdot (U \Phi) - \nabla \cdot \left(\left(\rho D_\Phi + \frac{\mu_t}{Sc_t} \right) \nabla \left(\frac{\Phi}{\rho} \right) \right) = S_\Phi \quad (4-4)$$

A very low value of kinematic diffusivity equal to 10^{-11} m²/s is specified for the additional variable. In CFX, turbulent viscosity is calculated as:

$$\mu_t = C_\mu \rho \frac{k^2}{\epsilon}$$

Where,

$$C_\mu = 0.09$$

k and ϵ are obtained by solving the turbulence kinetic energy and dissipation equations respectively. The default turbulent Schmidt number in CFX-5 is 0.9. You can modify this value with the solver expert parameter "turbulent schmidt number" (personal correspondence with CFX technical support). The default value of turbulent Schmidt number is used for all the simulations.

4.1.3 Boundary conditions

The boundary conditions used are:

- 1) For both Lower and Upper Channels, fixed velocity boundary condition (2 m/s) is used. The choice of the velocity value was based on the assumption that Reynolds Number for general structured packing applications is less than 10,000 (Petre et al., 2003). The average Reynolds Number calculated by CFX was 5500, which ensures turbulent conditions, and also satisfies the above mentioned assumption. Also, in the experimental study of gas flow in two-sheet structured packing system, Stoter (1993) used a velocity of 2 m/s. A flat velocity profile is used with the entering flow normal to the boundary. Turbulence intensity equal to 0.037 and auto computed length scale is specified, which is used by the solver to calculate turbulence kinetic energy and turbulence dissipation. Additional variable (tracer mass fraction) is set to a value of

one at inlet of Upper Channel and zero at the Lower Channel inlet i.e. the tracer is introduced only at the Upper Channel inlet.

- 2) At both the outlets, zero relative static pressure boundary condition is used.
- 3) At walls, smooth, no slip wall boundary condition is specified. In CFX, the near wall region is approximated using scalable wall functions as opposed to standard wall functions. In CFX 5.4.1 and earlier versions, only standard wall functions were available. In CFX 5.5.1, both scalable and standard wall functions are available.

Two approaches are commonly used to model the flow in the near-wall region:

- The wall function method
- The Low-Reynolds-Number method, where the Navier-Stokes equations are solved up to the wall. Highly refined mesh is required to capture the rapid variation of variables in the near wall region.

In the wall function approach, the viscosity affected sublayer region is bridged by employing empirical formulas to provide near-wall boundary conditions for the mean flow and turbulence transport equations. These formulas connect the wall conditions (e.g. the wall shear stress) to the dependent variables at the near-wall grid node, which is presumed to lie in the fully developed region of the boundary layer. The major advantage of the wall-function approach is that it conserves the valuable computer resources, and it avoids the need to account for viscous effects in turbulence model (CFX-5.5.1 user manual).

The disadvantage with the standard wall functions is that they result in a singular solution at separation points. The scalable wall functions are based on the turbulence equation, and the singularity at the separation point is avoided by using a limiting value

of Y^+ (scaled distance from wall). The basic idea behind the scalable wall-function approach is to assume that the surface coincides with the edge of the viscous sublayer, which is defined to be at $Y^+ = 11$. This region is the intersection between the logarithmic and the near wall profile. The computed Y^+ is not allowed to fall below this limit. Therefore, all grid points are outside the viscous sublayer and all fine grid inconsistencies are avoided. The scaled velocity for scalable wall function is given as

$$u^* = c_{\mu}^{1/4} k^{1/4} \quad (4-5)$$

4.1.4 Initial conditions

All fields except for velocity were initialized using “Automatic” initial values. The “Automatic” setting sets the pressure equal to the operating pressure specified in the domain form, and all velocity components equal to zero.

4.1.5 Meshing

Unstructured meshing with tetrahedral volume elements is used for the simulations. Delaunary Surface Meshing mode is used for creating the surface mesh and the volume mesh is created from the surface mesh using Advancing Front Inflation (AFI) mode. Inflation is used in the near wall region with 5 inflation layers.

In near wall regions, boundary layer effects give rise to velocity gradients, which are greatest normal to the surface. Computationally efficient meshes in these regions require that the elements have high aspect ratios. If tetrahedral elements are used, then a prohibitively fine surface mesh may be required to avoid generating highly distorted tetrahedral elements at the surface. This problem can be overcome by using inflation in

the near wall region. In the inflated layers prisms are used to create a mesh that is finely resolved normal to the wall, but coarse parallel to it. This mesh arrangement is beneficial for cost effective CFD analysis. The AFI volume mesher can use the local surface element normals to inflate 2D triangular surface elements into 3D 'prism' elements at selected walls or boundaries. Figure 4-7 shows the near wall meshing with inflation. The creation of these elements can be controlled using Inflation Parameters to determine their size and distribution in near-wall regions(CFX-5.5.1 user manual). Mesh generated for the base case is shown in Figure 4-8, where close to the wall, five layers of inflated mesh elements are present, and rest of the volume is filled with tetrahedral elements (unstructured mesh).

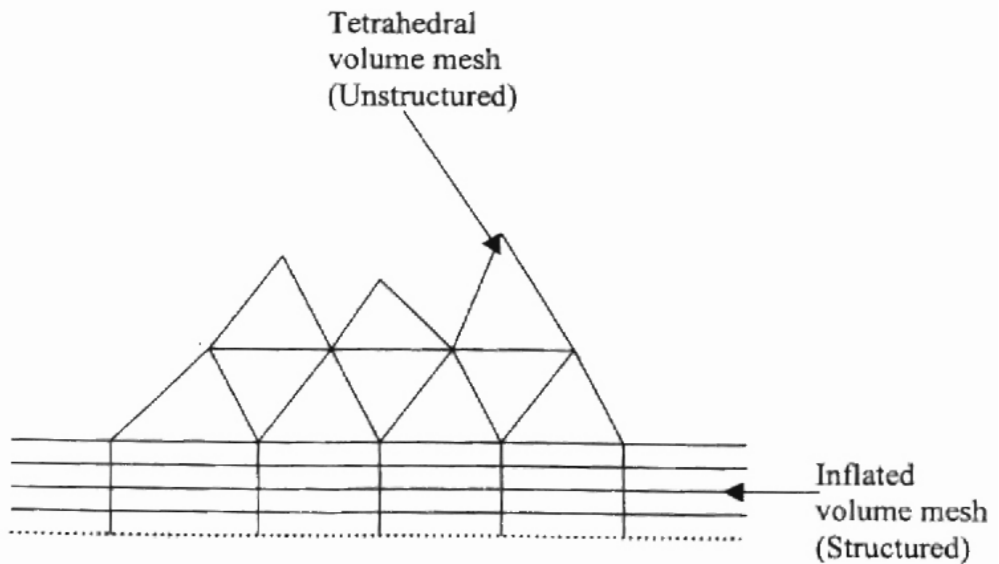


Fig 4-7 Volume mesh with inflated mesh elements in the near wall region

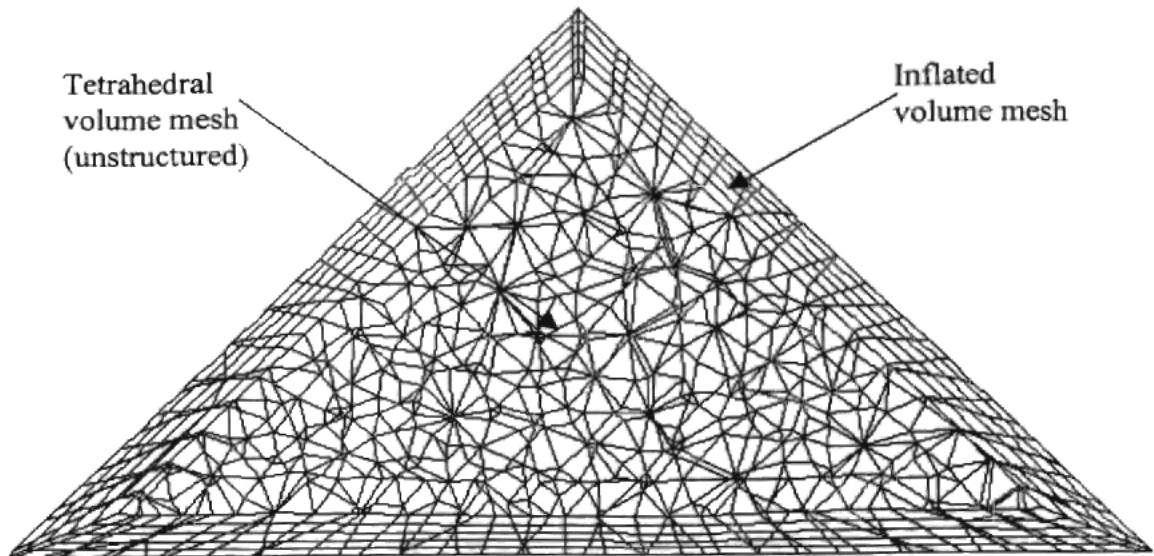


Fig 4-8 Mesh for the base case

4.1.6 Solver parameters

Maximum number of time steps = 100

Time step = Auto time step

(Auto time step is calculated as the ratio of cube root of the domain volume and velocity specified at the inlet)

Convergence criterion = 10^{-5} Normalized Root Mean Square (RMS) value

Advection scheme = *Second order High Resolution Scheme* was used to achieve near second-order accuracy

To complete the discretization of the advection term, the variable must be related to the nodal values of ϕ . The advection schemes implemented in CFX-5 can be cast in the form:

$$\phi_p = \phi_{up} + \beta \nabla \phi \cdot \Delta r' \quad (4-6)$$

Where, ϕ_{up} is the value at the upwind node, $\nabla\phi$ is the gradient of ϕ , and r' is the vector from the upwind node to ϕ_p . Particular choices for β give rise to different schemes. The High Resolution Scheme computes β locally to be as close to 1 ($\beta=1$ in Equation 4-5 will result in 2nd order scheme) as possible without violating boundedness principles. The high resolution scheme is therefore both accurate (reducing to first order near discontinuities and in the free stream where the solution has little variation) and robust.

4.1.7 Convergence

A typical convergence plot obtained for the base case is shown in Figure 4-9 and 4-10. The simulation took 178 iterations and a CPU time of 3 hours to converge.

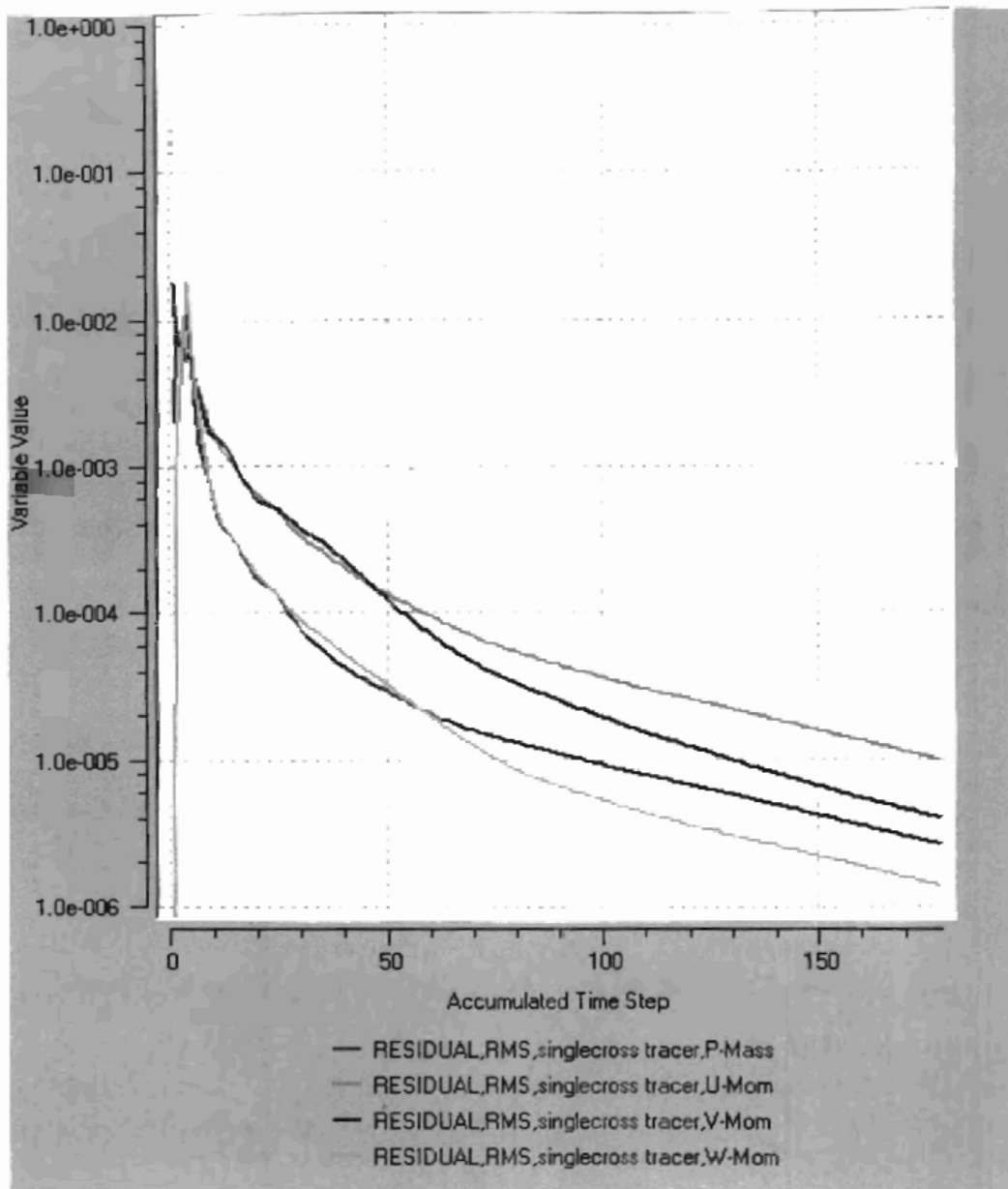


Fig 4-9 Residual plot for mass and momentum equations

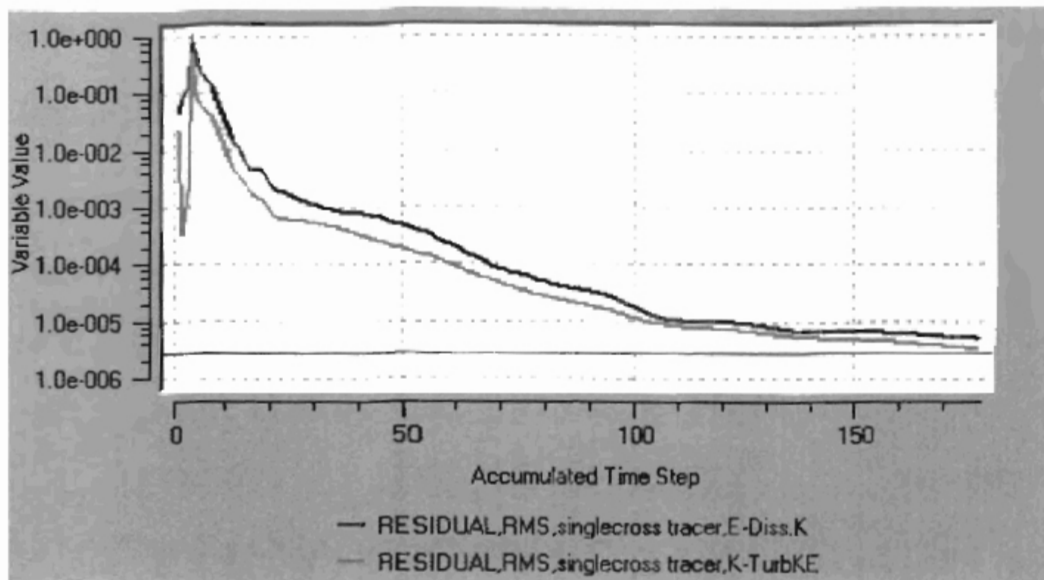


Fig 4-10 Residual plot for turbulence equations

The residual plots show a smooth convergence.

4.1.8 Results for the base case

Figure 4-11 shows the streamline plot (also streakline or pathline plot, since the simulation is a steady state simulation) for the two intersecting triangular channels. Red streamlines represent the flow path for the fluid entering from the Upper Channel inlet and blue for the Lower Channel inlet. The streamlines are plotted as constant color lines, and the color does not indicate any value. The flow from the Upper Channel inlet gets split at the intersection zone. Part of the flow goes straight (Upper Channel), and rest of the flow bends at 90° to enter the Lower Channel. Similar flow behavior is observed for the flow entering from Lower Channel inlet. The fraction of the flow bending at 90° is expected to result in a recirculation zone because of flow separation. For the flow entering from the Upper Channel inlet, the recirculation zone is expected to be developed in the circled portion shown in Figure 4-11. The vector plot, in Figure 4-12, shows the recirculation zone that is developed in this region. In the vector plot, red color indicates maximum velocity, blue indicates minimum, and rest represents the intermediate values.

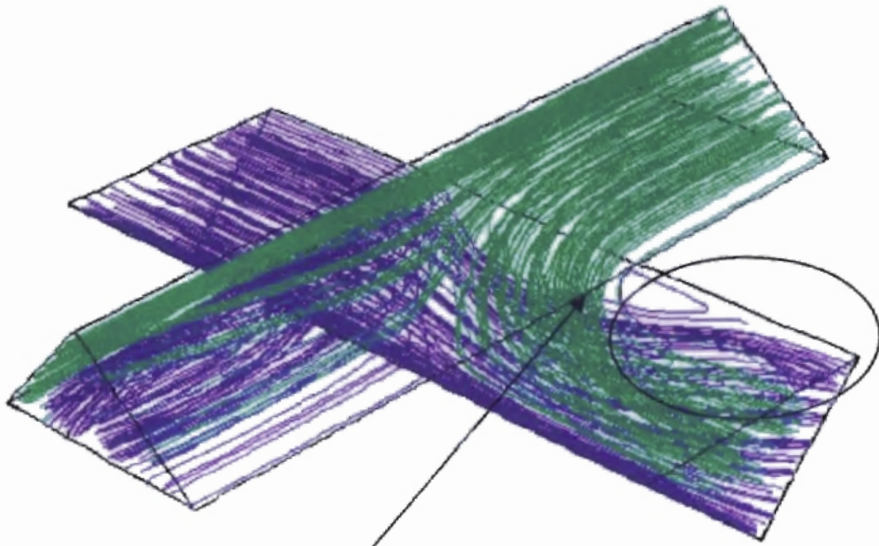


Fig 4-11 Streamline plot

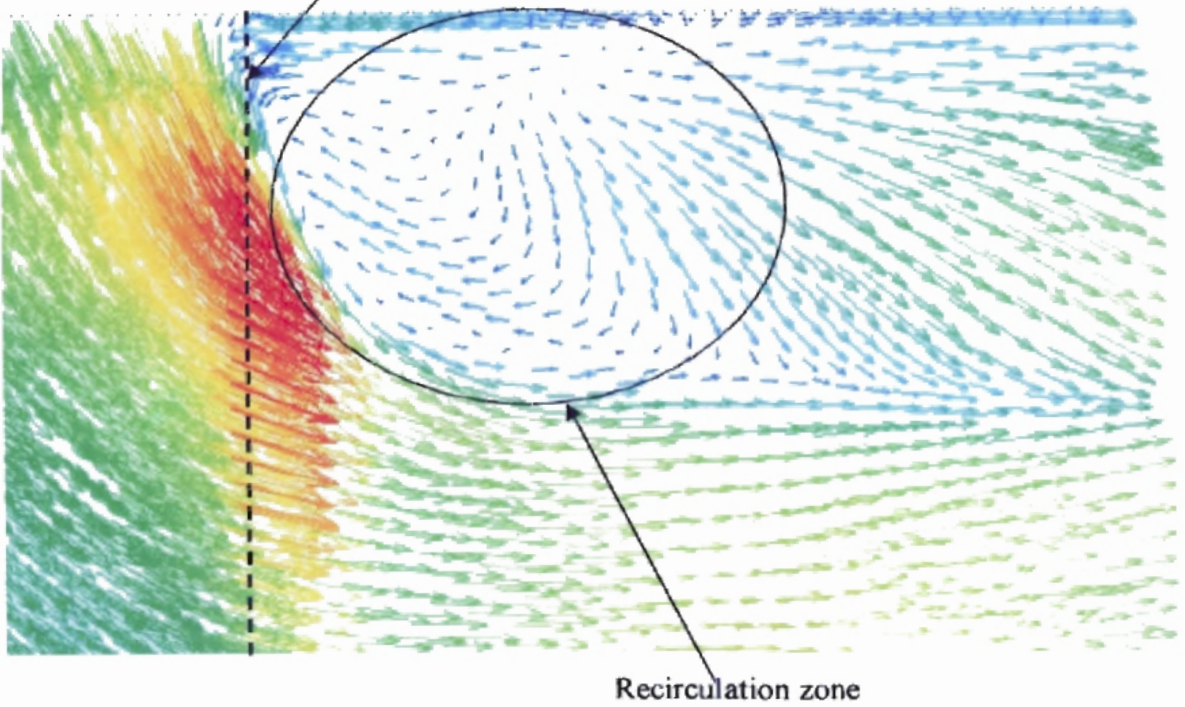


Fig 4-12 Vector plot for the circled region in Figure 4-11

Figure 4-13 shows the contour plot for tracer mass fraction distribution, and the “Mixing Band” within which the mass fraction is changing from zero to one. The contour plot for Figure 4-13 is shown on a plane at the center of the intersection zone. In Figure 4-13, the contour lines can’t be seen distinctly. Therefore an expanded view of the circled portion in Figure 4-13 is shown in Figure 4-14. Figure 4-15 shows the contour plot at the Upper Channel outlet. In Figure 4-15, the “Mixing Band” is spread over a larger area as compared to Figure 4-13 (see the Upper Channel portion of Figure 4-13), indicating an increase in mixing. The increase in mixing can be ascribed to the increase in interaction between flow streams from channels of adjacent sheets (Upper and Lower Sheet for the base case). For Figure 4-15 and all other tracer distribution contour plots, coming after this, refer to the Legend shown in Figure 4-13. A Legend represents the values corresponding to the colors used in the CFD results. For Figure 4-13, the Legend is shown on the extreme left hand side.

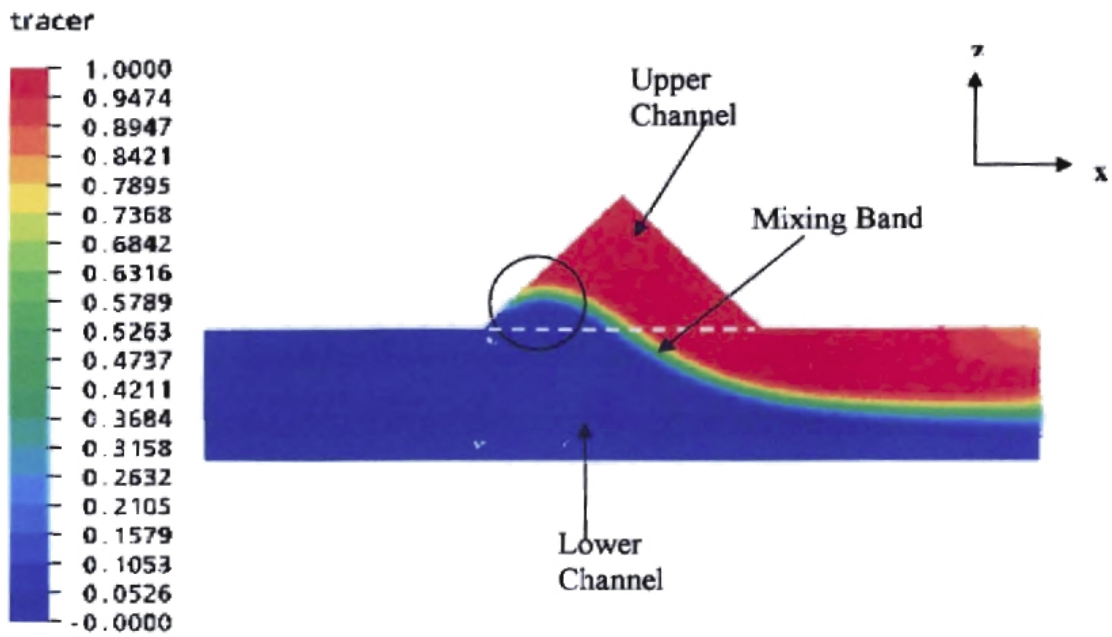


Fig 4-13 Contour plot for tracer mass fraction at the center of the intersection zone

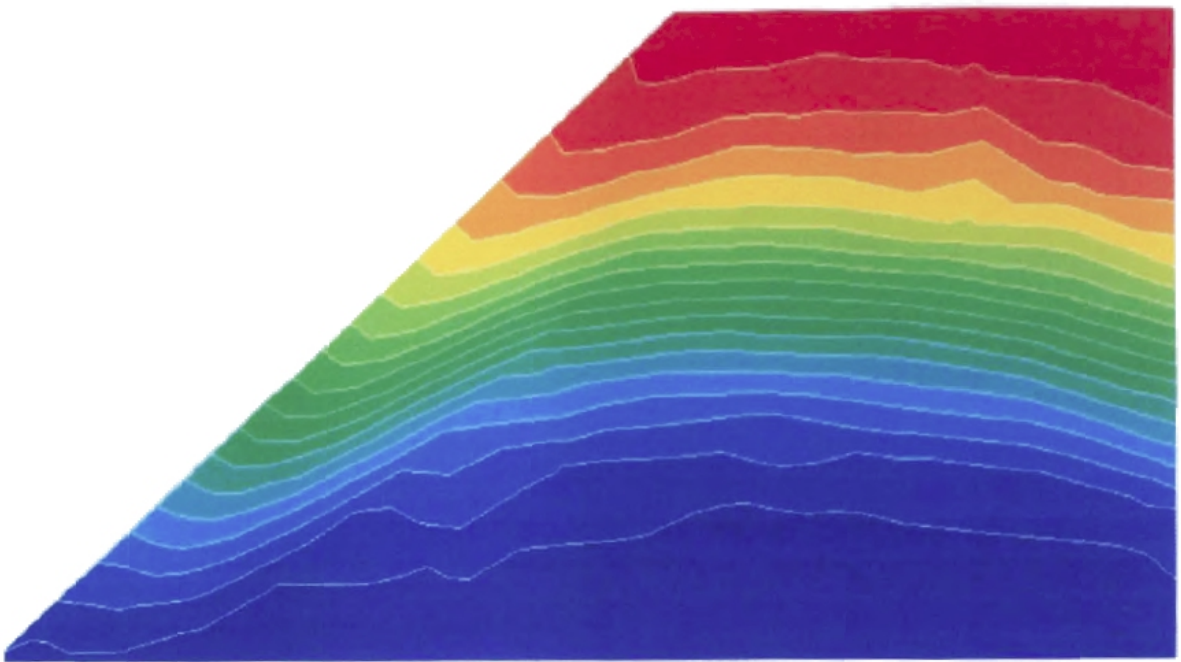


Fig 4-14 Expanded view of encircled portion in Figure 4-13

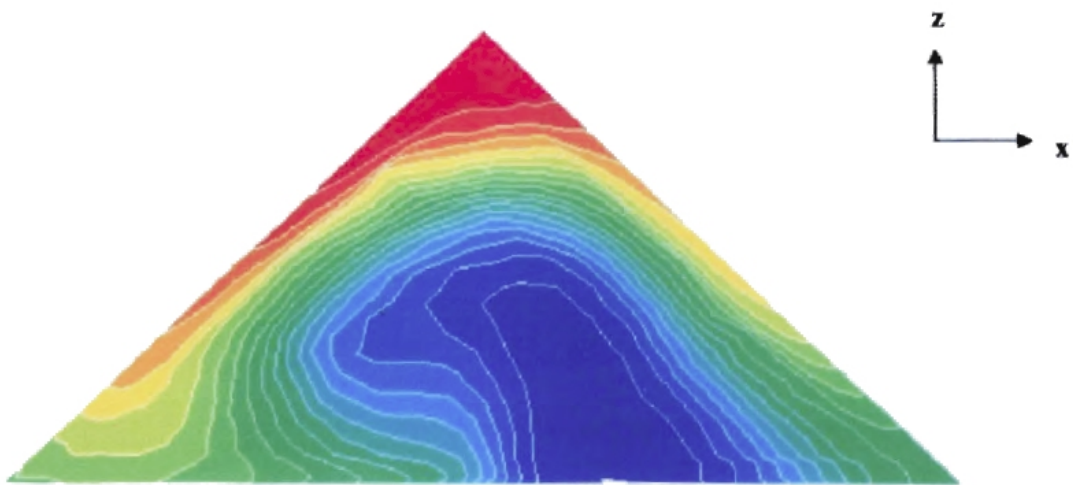


Fig 4-15 Contour plot for tracer mass fraction at Upper Channel outlet

(I) Effect of advection scheme selection

Sensitivity of the CFD results to the advection schemes was studied for the base case. Figure 4-16 and 4-17 show the results obtained using 1st order/Upwind Advection Scheme and Second Order High Resolution Scheme respectively, for the same mesh and boundary conditions. Figure 4-16 shows a spread out “Mixing Band” as compared to Figure 4-17. The reason behind the wider “Mixing Band” is the *numerical diffusion* associated with 1st order advection scheme. Numerical diffusion is usually exhibited by difference equations where the advection term has been approximated using an odd-order scheme, for instance, Upwind Differencing Scheme (UDS), which is first order accurate. The effect of the numerical diffusion over the whole flow domain is that the features of the flow are smeared out as observed in Figure 4-16. It is a fact that using the UDS scheme with tetrahedral element meshes will produce solutions that exhibit a larger degree of numerical diffusion than would exist from a solution obtained with a similar mesh of hexahedral elements. However, this discrepancy diminishes rapidly as the advective discretization is made more second-order accurate, and by working towards a grid independent solution (CFX-5.5.1 user manual).

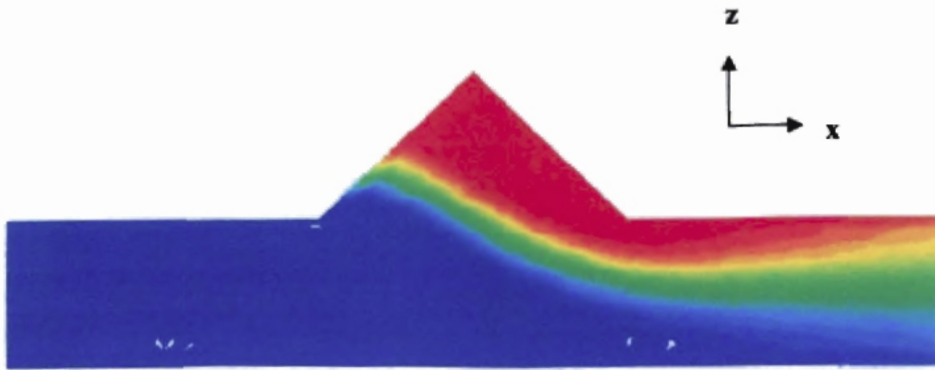


Fig 4-16 Contour plot for tracer mass fraction at the center of the intersection zone (using first order advection scheme)

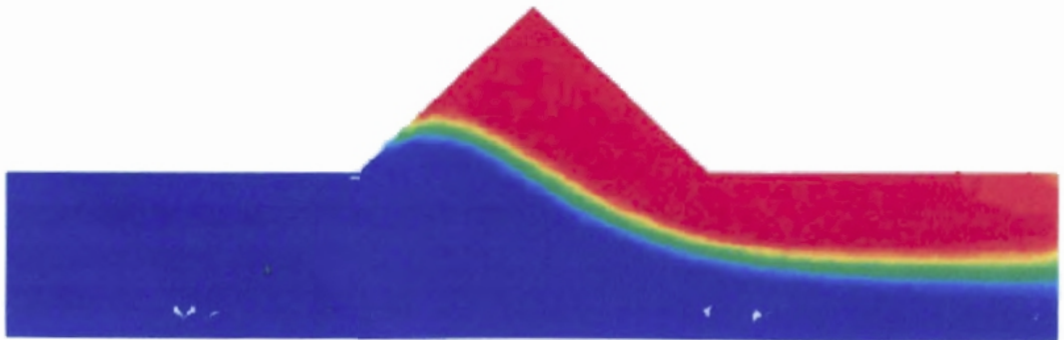


Fig 4-17 Contour plot for tracer mass fraction at the center of the intersection zone (using Second Order High Resolution Advection scheme)

(II) Effect of mesh size

A very low value of kinematic diffusivity equal to 10^{-11} m²/s is specified for the additional variable so that no mixing should occur because of diffusion. But, correspondence with the CFX technical support indicated that this argument is not entirely true. Setting the kinematic diffusivity to a small value will only prevent mixing if the flow is parallel to the *grid*. Since an unstructured mesh is used in the simulations, this will not be the case and some mixing will occur because of numerical diffusion. The level of numerical diffusion will increase with increased mesh size. So, a finer mesh will help in reducing the errors caused by numerical diffusion. To verify this fact, three different grid sizes were used to analyze the effect of mesh size on solution. The number of tetrahedral and prismatic elements for each mesh size is given Table 4-1.

	Tetrahedral elements	Prismatic elements
Mesh I	62501	36691
Mesh II	151151	69105
Mesh III	307411	108732

Table 4-1

The numbers for tetrahedral and prismatic elements are obtained from the solver output file. Results for each mesh size are shown in Figures 4-18 through 4-23. The effect of mesh size is seen more clearly in Figures 4-21 through 4-23. From Mesh I to Mesh III, the mesh size is reducing. From Figures 4-18 through 4-20, it can be observed that the spread of the Mixing Band is decreasing as the mesh size is decreasing i.e. the coarse

mesh is over predicting the mixing. Reducing mesh size has minimized this over prediction caused by numerical diffusion. All the CFD results for the base case are obtained with Mesh III.

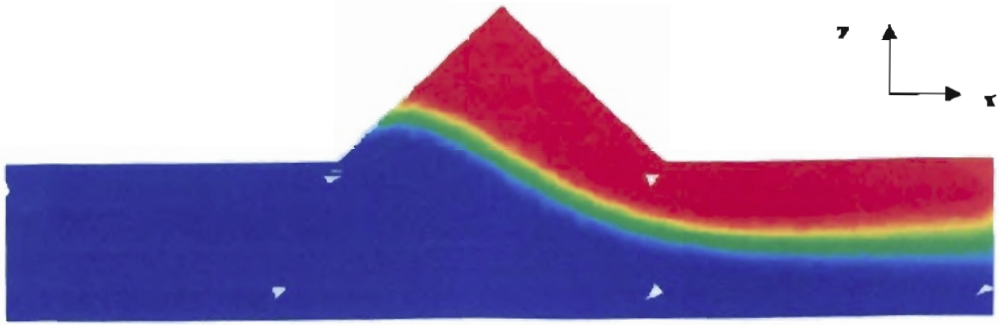


Fig 4-18 Contour plot for tracer mass fraction at the center of the intersection zone (for Mesh I)

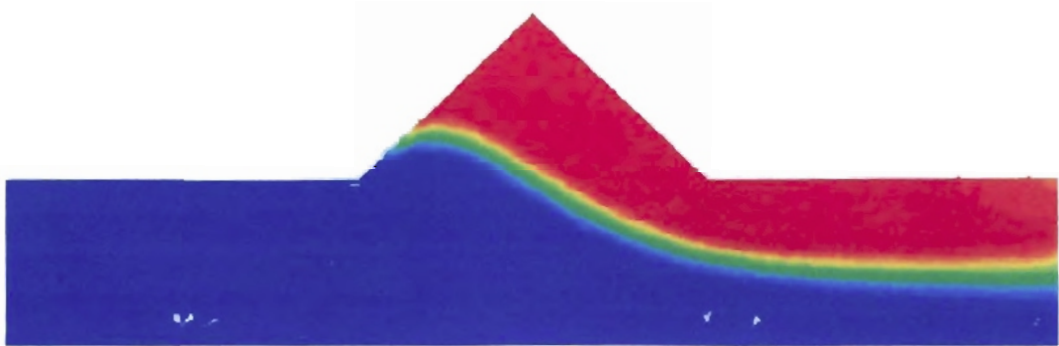


Fig 4-19 Contour plot for tracer mass fraction at the center of the intersection zone (for Mesh II)

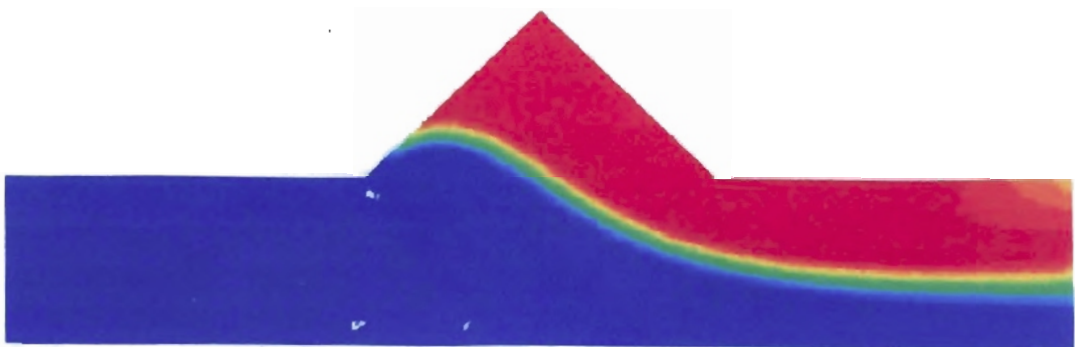


Fig 4-20 Contour plot for tracer mass fraction at the center of the intersection zone (for Mesh III)

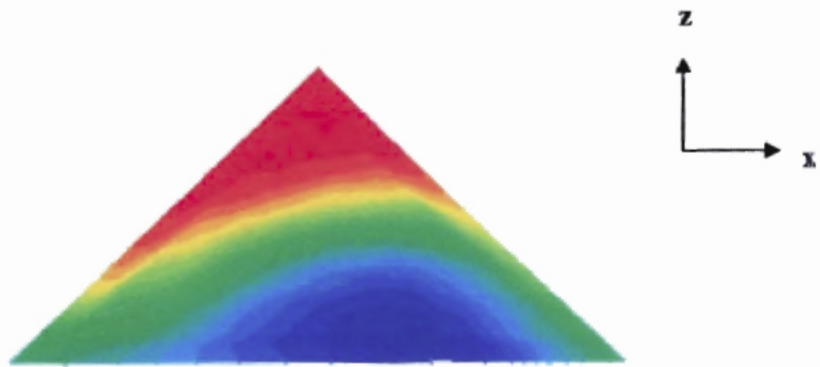


Fig 4-21 Contour plot for tracer mass fraction at Upper Channel outlet (for Mesh I)

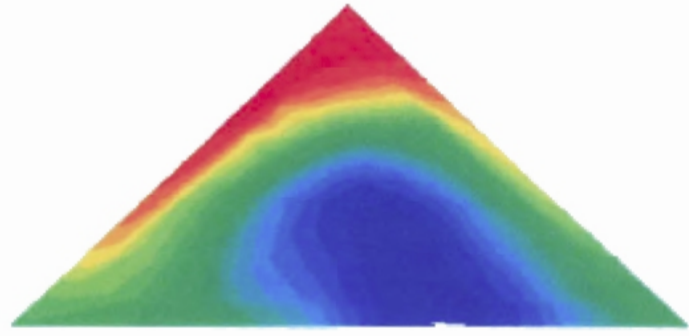


Fig 4-22 Contour plot for tracer mass fraction at Upper Channel outlet (for Mesh II)

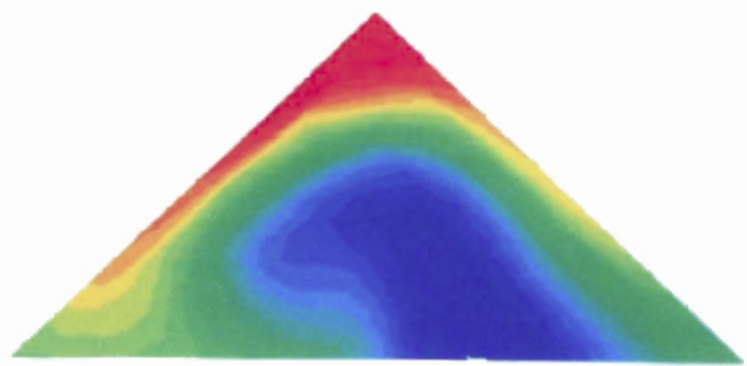


Fig 4-23 Contour plot for tracer mass fraction at Upper Channel outlet (for Mesh III)

(III) Splitting Factor

As shown in Figure 4-11, the flow in each channel gets split at the intersection zone with a fraction of the flow following the path of the channel, and remaining flow entering the channel of the adjacent sheet. Thus, the portion of each channel, downstream of the intersection zone, represents the mixing of two flow streams. “Splitting Factor” is defined as the fraction of the flow splitting at the intersection zone and entering the channel of adjacent sheet. For example, for the base case, Splitting Factor is the fraction of the flow in the Upper Channel entering the Lower Channel, which represents the adjacent sheet (same is true for flow in Lower Channel). Splitting Factor can be considered as the degree of flow mixing in a structured packing block consisting of sheets, stacked adjacent to each other.

(IV) Effect of turbulence intensity

Turbulence intensity (T.I.) needs to be specified as a part of inlet boundary condition. Since no experimental data was available for inlet T.I., effect of T.I. on performance parameters was studied so as to select appropriate T.I.. Two performance parameters, Splitting Factor and pressure drop, were chosen to evaluate the effect of T.I. Splitting Factor i.e. mass fraction of tracer at Lower Channel outlet is taken as a mass flow average value. Both pressure drop and tracer mass fraction are calculated using the calculator function in CFX POST. 0.001 and 0.1 are the lower and upper limits of T.I. that are allowed in CFX. As per CFX manual, normally T.I. ranges between 1-5%, and considering the fact that variation of both the parameters with T.I. is small (as can be inferred from Table 4-2), a value of 0.037 was used for all the simulations.

Turbulence Intensity	Splitting Factor	Pressure Drop (Pa)
0.001	0.55	0.33
0.037	0.541	0.362
0.06	0.536	0.386
0.1	0.531	0.42

Table 4-2 Effect of turbulence intensity on performance parameters

(V) Mesh Adaptation

For the problem studied in this thesis, it has been identified that numerical diffusion errors will result in over prediction of mixing at the intersection zone (based on the results in Section 4.1.8 (I and II)). Using a fine mesh and High Resolution Advection Scheme, the numerical diffusion errors are reduced as described in sections 4.1.8 (I and II). The tracer mass fraction is changing from 0 to 1 in only a small region (Mixing Band), and the error caused by numerical diffusion can be further reduced if a refined mesh is used in the Mixing Band. This selective mesh refining can be achieved by using Mesh Adaptation. Mesh Adaptation in CFX-5 is the process in which, once or more during a run, the mesh is selectively refined in areas, which depend on the Adaptation criteria specified. This means that as the solution is calculated, the mesh can *automatically* be refined in locations where solution variables are changing most rapidly, in order to resolve the features of the flow in these regions. For the base case, the mesh is adapted with the tracer mass fraction. Within the Mesh Adaptation step itself, three processes take place:

1. Adaptation Criteria are calculated for each mesh element.
2. The appropriate number of nodes is added to the existing mesh according to the Adaptation Criteria calculated.
3. The solution already calculated on the older mesh is linearly interpolated onto the new mesh.

The Mesh Adaptation algorithm is shown in Figure 4-24.

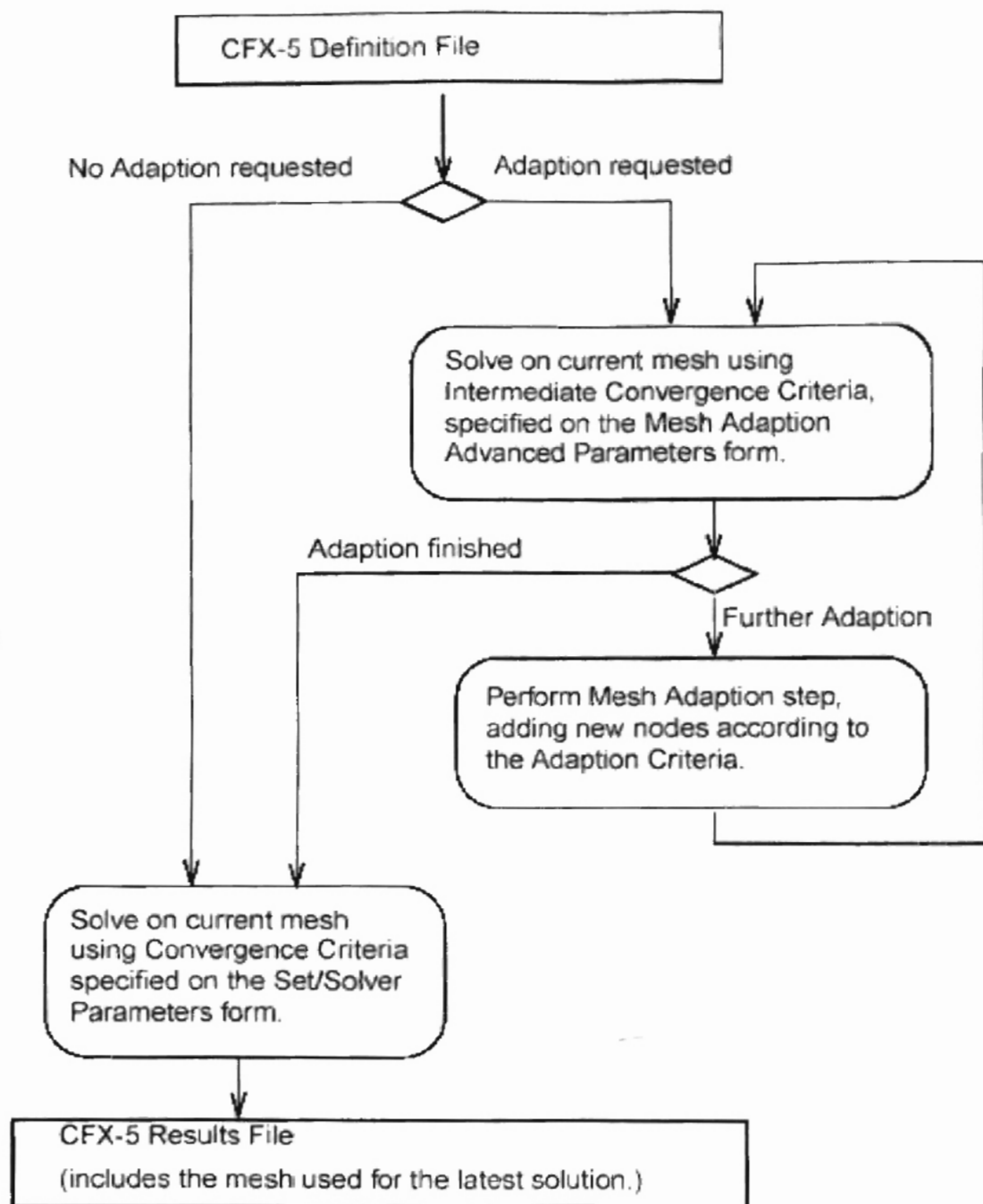


Fig 4-24 Flow chart for Mesh Adaptation in CFX-5 (reproduced from CFX-5.5.1 user manual)

For the base case, *Solution variation* is used as the Adaptation criterion, mathematical details of which are given below.

The Adaptation Criterion, A_i , for a given mesh edge i of length l_i is calculated as

$$A_i = \sum_j \frac{|\Delta\phi_{ji}|}{N_{\phi_j} |\Delta\phi_j|}$$

Where ϕ_j is the j^{th} Adaptation variable (e.g. density, pressure etc.), $\Delta\phi_j$ is the global range of the variable ϕ_j over all the nodes (excluding those on Wall boundary conditions for turbulent flow), $\Delta\phi_{ji}$ is the difference between ϕ_j at one end of the edge and the other end, and N_{ϕ_j} is a scalar for Adaptation variable ϕ_j to scale all the A_i to take values between 0 and 1. If you select more than one variable, then Adaptation Criterion are calculated and normalized for all of the solution variables selected at each element, and the maximum of these is used to decide whether to refine the element. You need to ensure that the variables you select will vary during the calculation; for instance, you should not select density for an incompressible flow calculation.

CFX-5 uses *incremental Adaptation* for mesh Adaptation. The particular implementation of incremental Adaptation that is adopted in CFX-5 is known as **hierarchical refinement** or **h-refinement**. Each Adaptation step consists of a structured refinement of an existing mesh. A sequence of refinements forms a set of hierarchical levels. In each Mesh Adaptation Step, each mesh edge, which is marked for Adaptation, has an extra node placed halfway along it. The mesh elements, which share this edge, are then divided to use the new node, and are subjected to the following restrictions:

- Neighboring elements must only differ by one refinement level. Hence, one mesh element cannot be divided twice if its neighbor has not been divided at all.
- Where possible, regular refinement of an element takes place. Regular refinement means that all the edges of an element are divided into two, and the element split accordingly. To make this possible, extra nodes may be added.
- No “hanging” nodes are allowed. This means that if an extra node is added to an edge, all the mesh elements, which share that edge, must be refined.
- Only certain types of elements are allowed in the refined mesh: tetrahedron, prism, pyramid and hexahedron.

In regions where Inflation has taken place (so that there are prisms and some pyramid elements near Wall Boundary Conditions), the Mesh Adaptation avoids refining these elements in the direction perpendicular to the Wall. Only edges on the interface between the inflated elements and the rest of the tetrahedral mesh are allowed to be marked for Adaptation. When the refinement of these edges takes place, the refinement propagates through the layers of prismatic elements to the Wall Boundary Condition itself. For the base case, mesh inflation is used in the near wall region.

Adaptation parameters are specified on the “*set solver parameter*” form in CFX-BUILD. The Adaptation parameters used for the base case and significance of these parameters is given below.

- 1) **Adaptation Criterion:** Solution variation
- 2) **Adaptation variable:** Tracer mass fraction
- 3) **Maximum number of Adaptation steps:** 3

This sets the number of mesh Adaptation steps that take place. In CFX-5 user manual, it is recommended that you choose a number between 1 and 5.

4) Number of nodes in adapted mesh: Multiple of initial mesh = 3

This setting allows you to select how many nodes will be in the final mesh. You can either select *Final Number of Nodes*, which allows you to specify the number of nodes directly, or select *Multiple of Initial Mesh*, which allows you to specify the number of nodes in the final mesh as a multiple of the initial mesh. If you select *Multiple of Initial Mesh*, you must enter a multiplier which is greater than 1.2. If you select to specify *Final Number of Nodes*, then you are advised to choose a number of nodes, which is no more than a factor of five greater than the number of nodes in the initial mesh. For results presented in this section, *Multiple of Initial Mesh* option is used. The initial mesh used here is MESH III (refer Table 4-1). In setting up the Adaptation parameters, the tutorial “*Free surface flow over a bump*”, given in CFX-5.5.1 user manual, was referred.

Since the tracer mass fraction is varying between 0 and 1 in the Mixing Band, it is expected that during Mesh Adaptation mesh in the Mixing Band region will be refined. The mesh generated during the Adaptation steps is shown in Figures 4-25 and 4-26. Since the mesh for the third Adaptation step is same as that of second step, it is not shown here. Figure 4-25 i.e. mesh for the first Adaptation step is same as Mesh III, whereas Figure 4-26 shows the mesh after it is being adapted to the Adaptation variable i.e. tracer mass fraction. As expected, the mesh is refined in the Mixing Band region shown by the yellow band in Figure 4-26. The fact that same mesh is generated for Adaptation step 2 and 3 indicates that only two Adaptation steps will suffice for the base case.

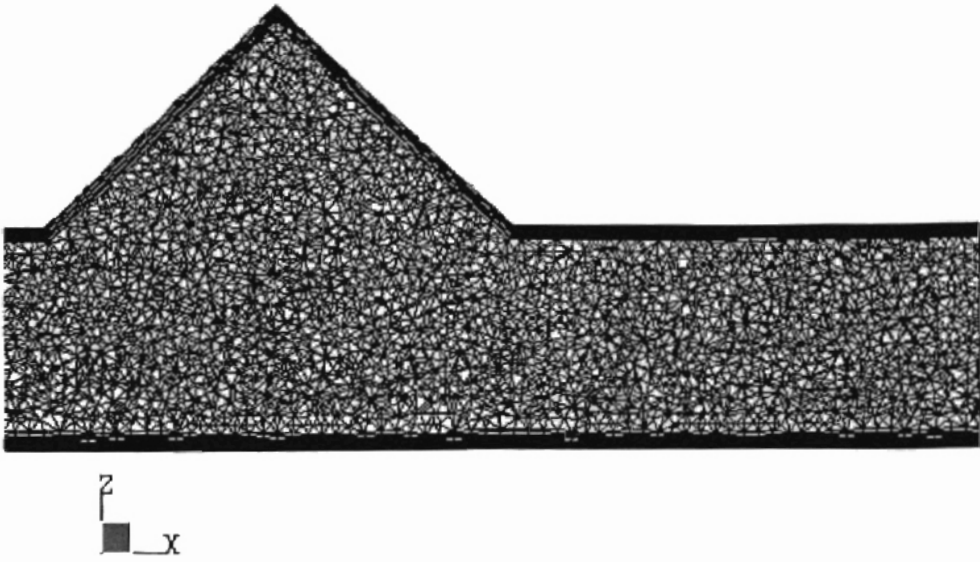


Fig 4-25 Mesh for the 1st Adaptation step

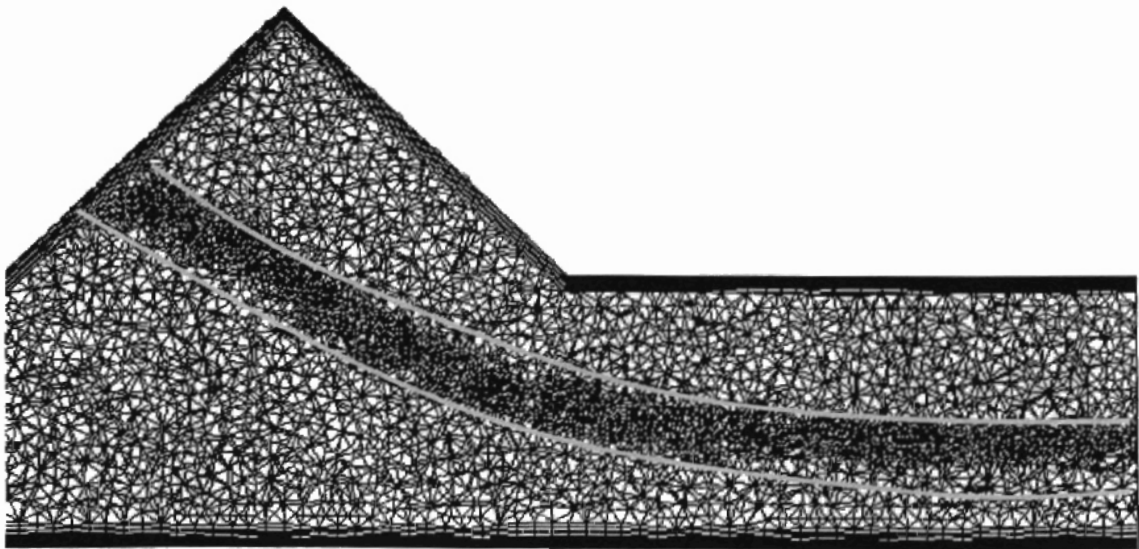


Fig 4-26 Mesh for the 2nd Adaptation step

Figures 4-27 and 4-28 show the contour plot for tracer mass fraction obtained for the first and second Adaptation steps. The contour plot for third Adaptation step was found to be same as that of second. This corroborates the fact that only two Adaptation steps are required. Comparing the Mixing Band spread in Figures 4-27 and 4-28, it can be observed that the over prediction of mixing, caused by numerical diffusion, is reduced further as a result of Mesh Adaptation. Therefore, it can be concluded that for simulations, which consist of mixing of flow streams, use

- Higher order advection scheme
- Refined mesh
- Mesh Adaptation

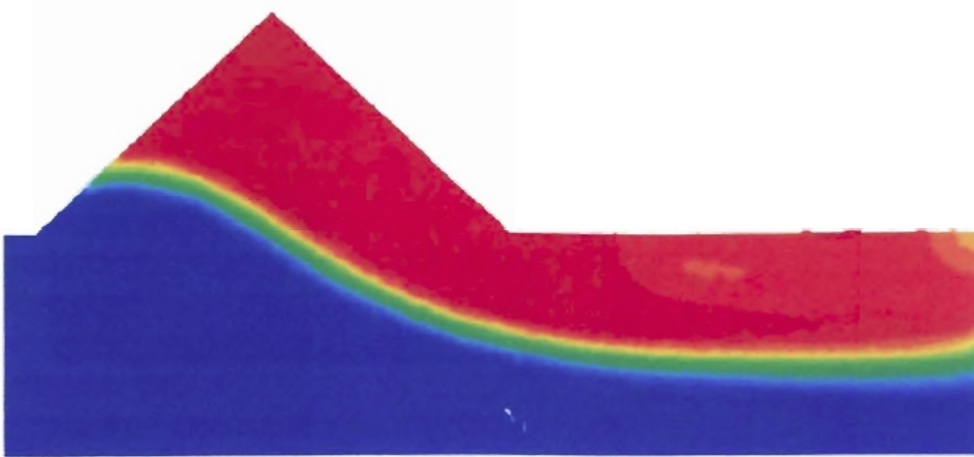


Fig 4-27 Contour plot for tracer mass fraction at the center of the intersection zone (1st Adaptation step)

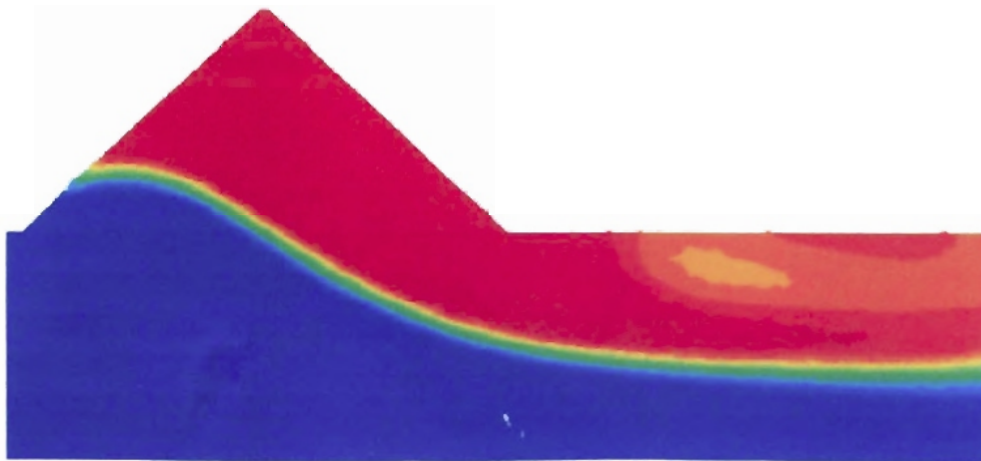


Fig 4-28 Contour plot for tracer mass fraction at the center of the intersection zone (2nd Adaptation step)

4.1.9 Comparison of the CFD results with experimental results (for base case)

In past, visualization experiments have been conducted to study the flow profiles in intersecting square ducts/ channels (Umeda et al., 1994;Zhang et al., 1993). To the best knowledge of the author, no experimental study has been done for intersecting triangular ducts. The geometry considered in this thesis is different from the one that has been studied in the literature, not only in terms of the shape (square and triangular cross section), but also the way the channels are aligned. Therefore, the flow physics associated with the two geometries is also different. . Figures 4-29 and 4-30 will make this point more clear. In both the figures, the intersection zone is shown by the circled region. Figure 4-29 shows the geometry studied in literature. In Figure 4-29, mixing at the intersection takes place by direct impingement of flows coming from both the inlets. Figure 4-30 shows the square shaped version of the base case geometry (as shown in Figure 4-4). In Figure 4-30, mixing at the intersection takes place because of the shear between the flows from upper and lower inlet. To the best knowledge of the author, no experimental study has been conducted for the geometry considered in this study.

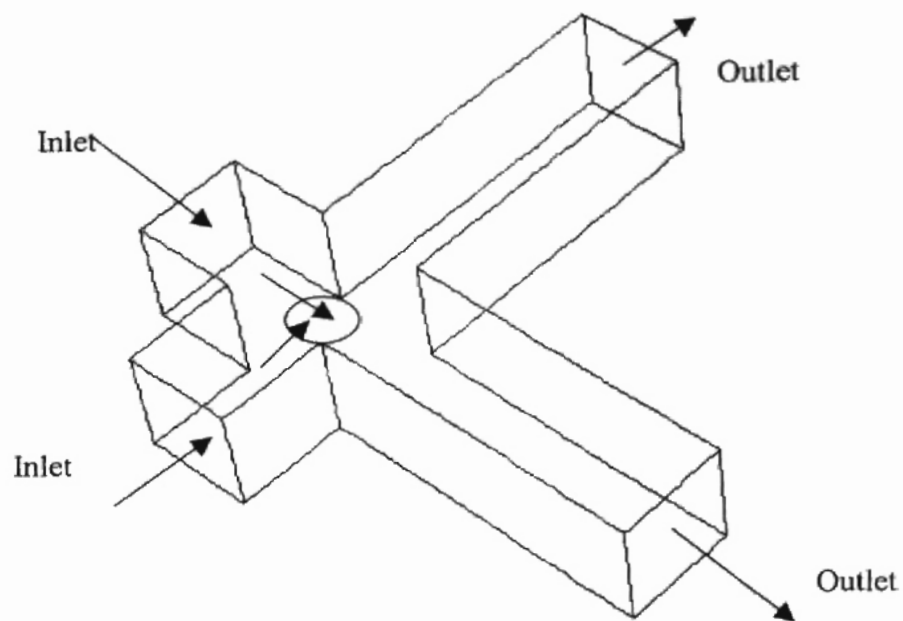


Fig 4-29 Geometry similar to the one that has been studied in the literature (Umeda et al., 1994;Zhang et al., 1993)

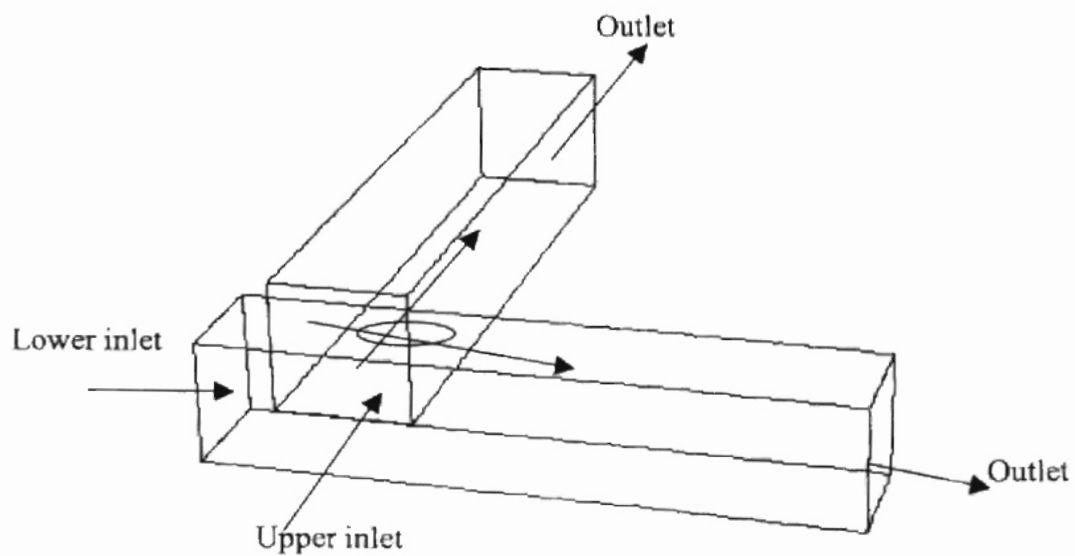


Fig 4-30 Geometry similar to the one that is being used in the this study

4.2 Effect of design parameters on the performance of structured packing

The sheets in a structured packing block are stacked in such a manner that the adjacent sheets have different channel orientation so that the channels intersect each other at an angle. The purpose of this type of design is to enhance the radial spread and mixing of the gas phase. Splitting Factor is a measure of mixing between flow streams. Pressure drop is a measure of the capacity of the packing. Packing capacity can be roughly defined as “the vapor velocity above which liquid accumulates uncontrollably in the packed bed and continued operation becomes impossible”. Packing with high pressure drop has low capacity. Pressure drop and Splitting Factor are chosen as performance parameters for this study. Channel inclination angle (θ) i.e. angle made by the channels with the horizontal and crimp angle (Φ) i.e. angle between the base and the side of the triangular cross section are the design parameters considered in this study.

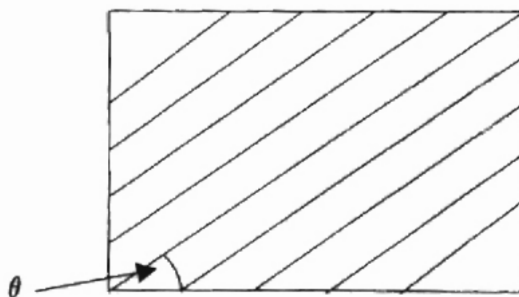


Fig 4-31 Structured packing sheet showing channel inclination angle (θ)

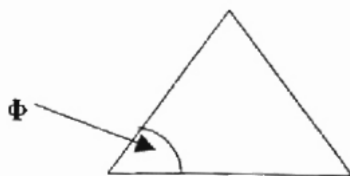


Fig 4-32 Channel cross section showing crimp angle (Φ)

4.2.1 Effect of channel inclination angle

The effect of channel inclination angle (also called as corrugation angle) on the performance parameters was studied by running simulations for a wide range of angles. The channel dimensions are same as that of base case; only inclination angle is varied. For the geometry used in this study, the channel inclination angle is shown in Figure 4-33.

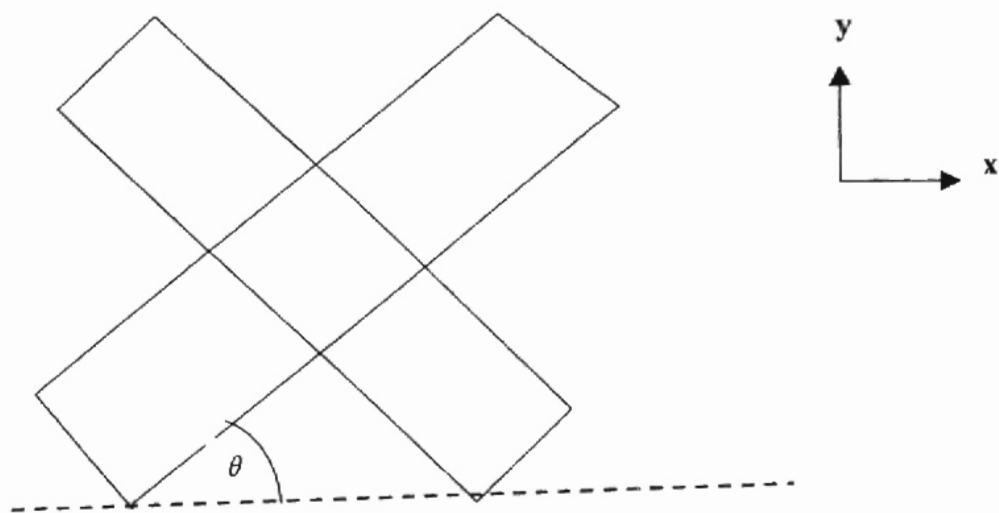


Fig 4-33 Location of channel inclination angle (θ)

Experimentally it has been observed that the mass transfer efficiency of the column decreases with the increase in the channel inclination angle (Olujic et al., 2000). However, the experimental study has not discussed any reasons for the decreased efficiency. Figure 4-34 shows that Splitting Factor decreases with θ i.e. mixing of the flow streams in a structured packing block decreases with θ . The decrease in gas mixing, caused by the increase in inclination angle, can be a probable cause for the observed decrease in column mass transfer efficiency.

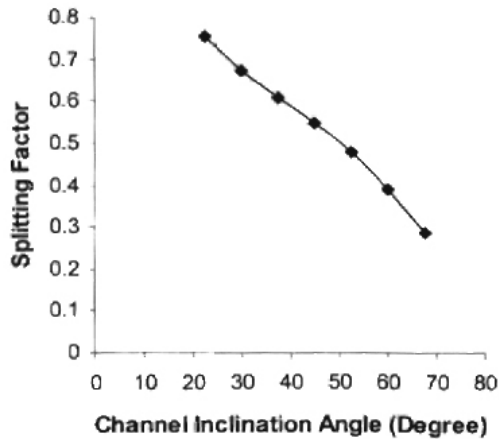


Fig 4-34 Splitting Factor as a function of channel inclination angle for a crimp angle of 45°

Figure 4-35 shows that pressure drop decreases with the inclination angle, which is in accordance with the experimental observations (Olujic et al., 2000; Petre et al., 2003). The pressure drop, in the problem under consideration, is caused by the interaction of two streams at the intersection. Total pressure drop in a structured packing bed is comprised of:

- Elbow loss and stream splitting in bed entrance region
- Pressure drop due to flow interaction at crisscrossing junctions (intersection)
- Elbow loss by form drag at the transition between successive layers
- Elbow loss by flow striking the wall and subsequent flow redirection to Upper Channels (Petre et al., 2003)

The pressure drop at the intersection contributes about 65-72% of the total pressure drop (Petre et al., 2003). Literature has strongly emphasized the need of reducing this pressure

drop as a part of developing efficient packing (Olujic et al., 2000). Decrease in pressure drop will result in increased packing capacity and reduced energy consumption.

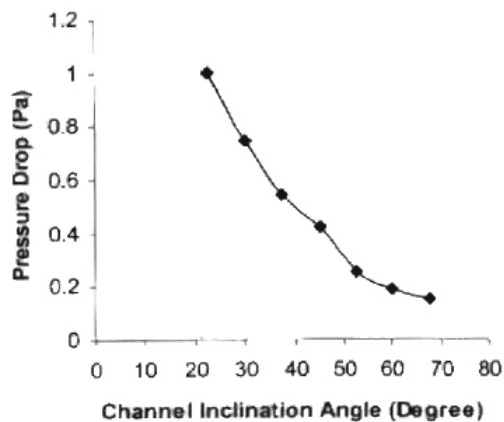


Fig 4-35 Pressure drop as a function of channel inclination angle for a crimp angle of 45°

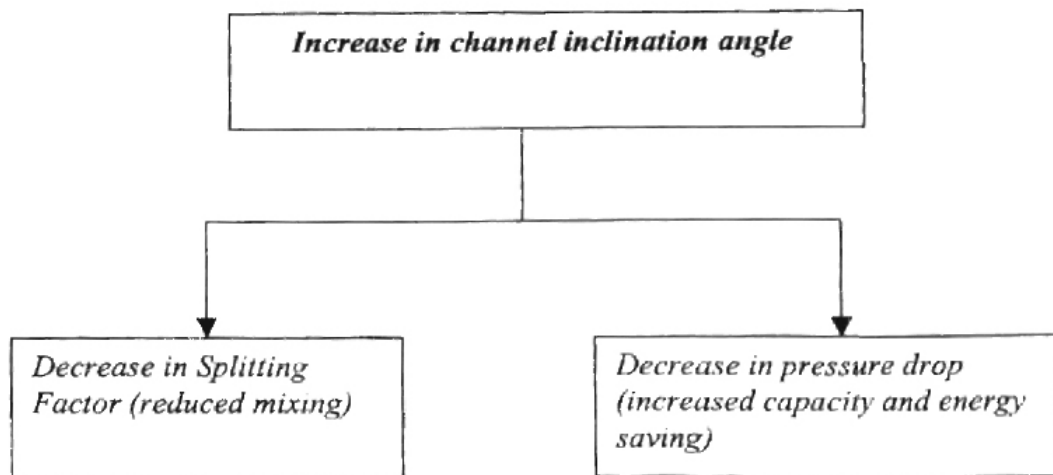


Fig 4-36 Effect of channel inclination angle on Splitting Factor and pressure drop

Therefore, while selecting a channel inclination angle for an efficient packing design, a balance between the two performance parameters has to be maintained.

4.2.2 Effect of crimp angle

Once the optimum channel inclination angle for the structured packing is chosen, another design parameter that can be varied, for a given inclination angle, is crimp angle. Figure 4-37 and 4-38 show that both Splitting Factor and pressure drop decrease with the increase in crimp angle. To the best knowledge of the author, there has not been any independent work published in the literature addressing the effect of crimp angle on packing performance. But, if the experimental data (Petre et al., 2003) for Gempak (crimp angle= 43° and inclination angle= 45°) and Montz B1-250 (crimp angle= 36.9° and inclination angle= 45°) for dry pressure drop is compared, it can be observed that pressure drop for Montz packing is greater than Gempak packing i.e. pressure drop decreases with the increase in crimp angle. This corroborates the CFD results shown in Figure 4-38. Similar trends are obtained with an inclination angle of 22.5° and three crimp angles that are tested for 45° inclination angle. Thus, for the reasons explained in section 4.2.1, a balance has to be maintained between the performance parameters while selecting optimum crimp angle.

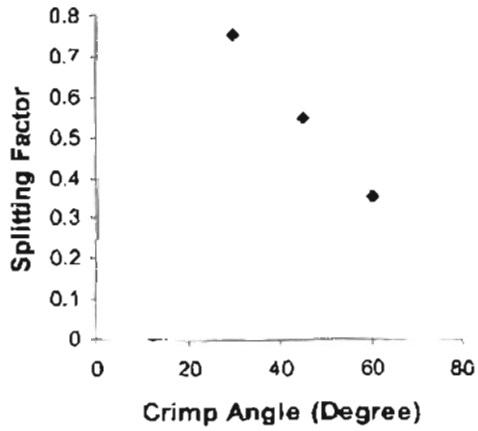


Fig 4-37 Variation of Splitting Factor as a function of crimp angle for a channel inclination angle of 45°

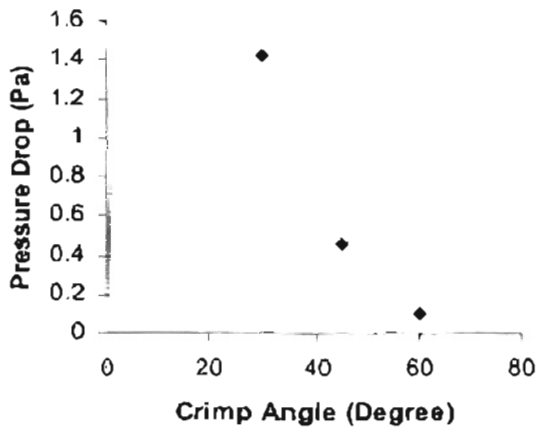


Fig 4-38 Variation of pressure drop as a function of crimp angle for a channel inclination angle of 45°

4.3 Effect of surface roughness

The CFD results presented in earlier sections were obtained with assumption of smooth walls. In reality, the surface of a structured packing sheet is roughened so as to improve the wettability and liquid turbulence. The smooth wall boundary condition for the single-phase flow is based on the assumption that the liquid film (in two-phase flow) on the sheet surface is thick enough so that the gas flow pattern will not be affected by the surface roughness. However, in case of liquid maldistribution, the gas phase will be exposed to rough surface (since no liquid film will be present on the surface). Thus, single-phase simulation with rough wall boundary condition was carried out. The roughness height was measured for the Mellapak™ packing, obtained from Fractionation Research Inc., Stillwater, using electronic Vernier Caliper. A value of 0.5 mm was specified as the roughness height. A careful mesh generation is required to capture the effects of roughness. Following suggestions were obtained from CFX technical support through personal correspondence:

- Use an epsilon based turbulence model (K-epsilon, RNG k-epsilon, or the RSM models based on epsilon). Omega based models do not work with surface roughness.
- The thickness of the first element off the wall should be about the same as the roughness height that you set. If the first element thickness is much less than the roughness height, then you would be attempting to resolve the wall roughness with the mesh. In this case, the rough wall assumption will not be valid. Also, as a rough guide, if the first element of the inflation (prismatic element) is about 5 times thinner than wall roughness, then y^+ can become negative which is invalid.

But, larger value of the first prism height will increase the value of Y^+ . So, a value of half the roughness height or close to that will be appropriate for the height of first prism in the inflated layer.

- The size of the prism cell bordering the unstructured tetrahedral mesh must be close to the tetrahedral cell dimensions to have a smooth transition from prisms to tetrahedrons. This smooth transition can be achieved by using a geometric expansion factor of 1.2 or less in the inflation parameter form of CFX-BUILD.
- Use Scalable Wall Function.

In accordance with the above suggestions, RNG k-epsilon turbulence model is used along with Scalable Wall Function. First prism height is set instead of maximum thickness of the inflation layer. The method of setting the first prism height does not control the overall height of the inflation layers, but creates prisms based upon the first prism height and the expansion factor. As a result, the Maximum Inflation Thickness setting is overridden and becomes unavailable. The setup involves specifying a first prism height and an expansion factor. The number of inflation layers then needs to be specified in relation to these two parameters and the background mesh spacing.

Successive layers of inflated elements will be created until either:

- The prism element reaches unit aspect ratio (same height as base length)
- The number of layers specified has been reached.

If the number of layers specified is too few to allow unit aspect ratio prisms to be created, a warning message will appear that contains a recommended number of layers. Conversely, if too many layers are specified a warning message will appear

recommending that you reduce the number of layers. The suggested number of layers depends on the Volume mesh spacing - maximum edge length. This method of inflation creates a smoother transition from the inflated prism mesh elements to the tetrahedral mesh elements (CFX-5.5.1 user manual).

For this simulation, the inflation parameters for the inflated boundary are:

- Number of layers = 24
- Geometric expansion factor = 1.15
- First prism height = 0.35 mm (roughness height is 0.5 mm)

The number of layers is the one that is being recommended by the warning message in CFX-BUILD as described above.

The mesh generated with these parameters is shown in Figure 4-39

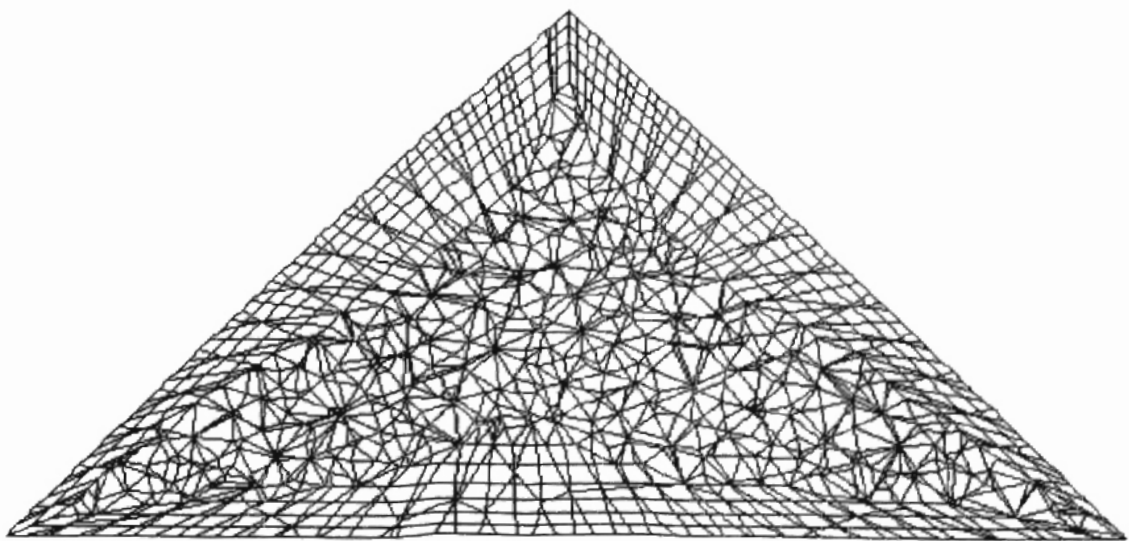


Fig 4-39 Mesh generated to study the effect of roughness

Figure 4-40 shows the contour plot for tracer mass fraction with rough walls. Figure 4-40 is not much different from Figure 4-20, which shows the contour plot for smooth wall. The only difference is the circled portion in Figure 4-40. The mass fraction variation in this region is more pronounced than Figure 4-20. The results in Figure 4-20 were obtained with 5 inflation layers, whereas for Figure 4-40, 24 layers were used. The meshes used for both these results are shown in Figures 4-41 and 4-42. This difference in mesh types, in the encircled portion, might be causing the results to vary. Therefore, to verify this argument, simulation for smooth wall boundary condition was carried out with the mesh used for rough wall (shown in Figure 4-42). Figure 4-43 confirms that difference in mesh types was causing the variation in results observed in Figures 4-20 and 4-40. Thus, CFD results indicate that wall roughness has no influence on tracer distribution. Same value of Splitting Factor was obtained for rough and smooth wall, which further corroborates this finding. Further study is required to confirm this prediction. Table 4-3 gives the pressure drop for the rough and smooth wall boundary conditions, where the mesh with 24 inflation layers was used for both the simulations. As expected, the pressure drop for rough wall is greater than smooth wall. But, the difference is not significant.

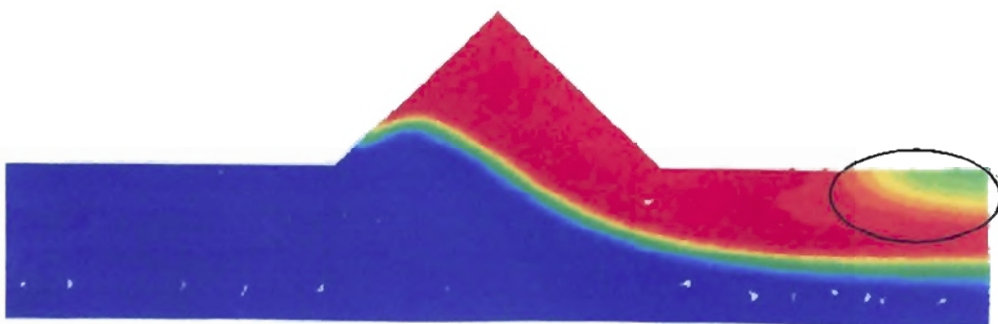


Fig 4-40 Contour plot for tracer mass fraction at the center of the intersection zone

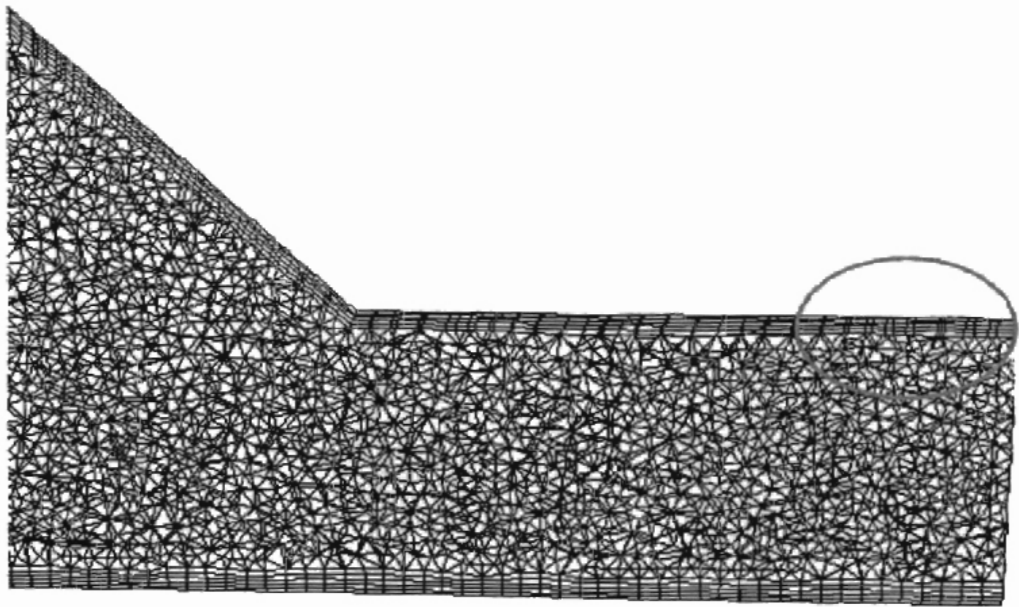


Fig 4-41 Mesh generated with 5 inflation layers (the result obtained with this mesh is shown in Figure 4-20)

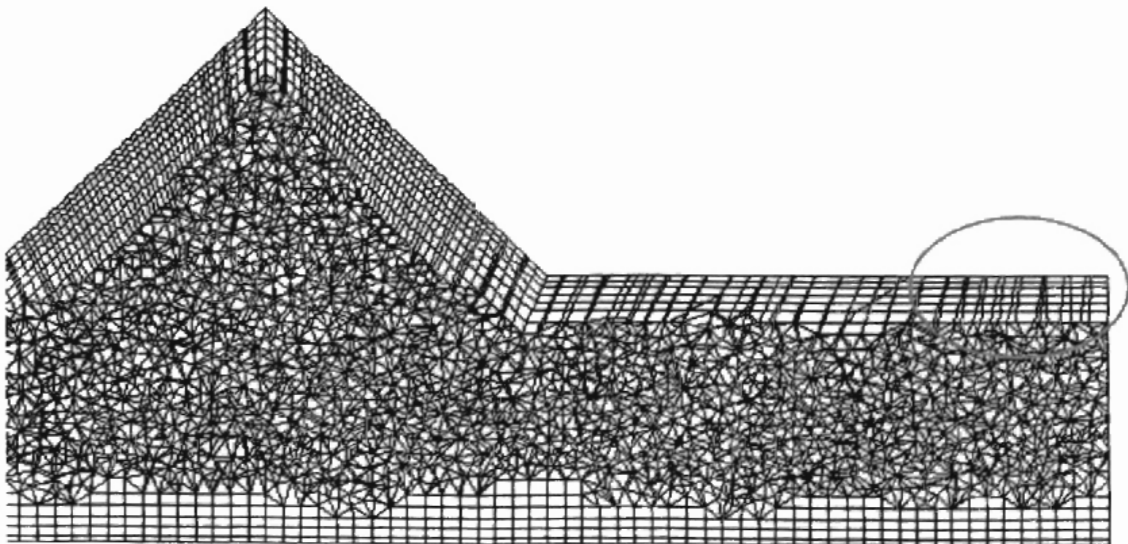


Figure 4-42 Mesh generated with 24 inflation layers (the result obtained with this mesh is shown in Figure 4-40)

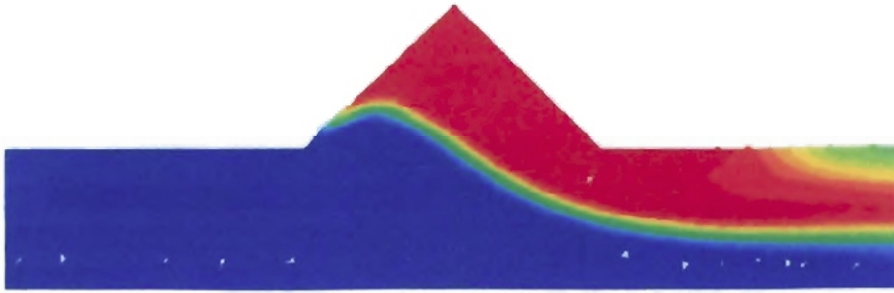


Fig 4-43 Contour plot for tracer distribution at the center of the intersection zone (For smooth wall with 24 inflation layers)

Wall boundary condition	Pressure drop (Pa)
Smooth	1 394
Rough	1.5

Table 4-3 Effect of wall boundary condition on pressure drop

4.4 Effect of inlet boundary condition

So far, all the simulation results presented are based on the assumption of equal velocity at both the inlets. This assumption is based on uniform vapor distribution in the structured packing block, and represents an idealistic situation. In reality, vapor maldistribution takes place i.e. velocities are different at the inlets. Therefore, simulations were carried out for the base case geometry with different velocities specified at Upper and Lower Channel inlets. Results in Figure 4-44, and 4-45 and 4-46 are obtained with velocities equal to 1.5 m/s and 1 m/s respectively at Lower Channel inlet. In both cases, velocity at the Upper Channel inlet is 2 m/s. The mesh used is Mesh III, details of which are given in Section 4.1. Rest of the parameter specifications is same as that of the base case. Comparing Figure 4-20 (with equal velocities at both the inlets) with Figures 4-44 and 4-45, it can be observed that in the intersection zone (bounded by dotted lines in Figure 4-44), there is not much change in the Mixing Band. Although, the curvature of the mixing band in the intersection zone for Fig 4-45 is less than 4-20 and 4-44, the width remains almost the same. Downstream of the intersection zone, a large change in the Mixing Band is observed. Splitting Factor decreases with the decrease in the velocity at the Lower Channel inlet as shown in Table 4-4 i.e. less flow from the Upper Channel inlet is entering the Lower Channel at the intersection zone. This type of flow pattern is expected to be seen in actual structured packing operation, where vapor maldistribution takes place.

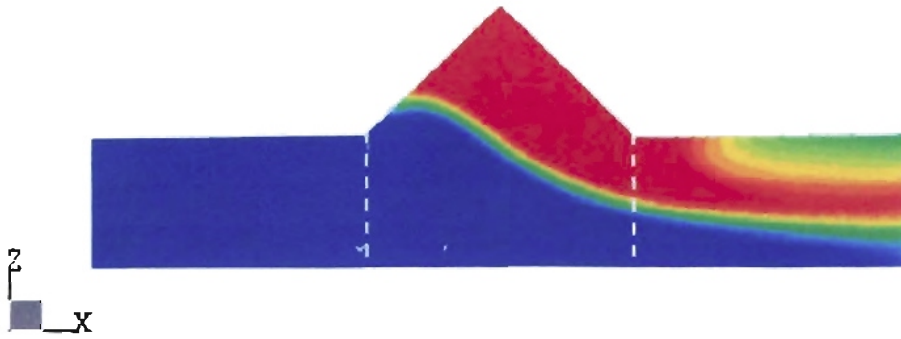


Fig 4-44 Contour plot for tracer distribution at center of the intersection zone (Velocity at Lower Channel inlet=1.5 m/s and Upper Channel Inlet = 2 m/s)

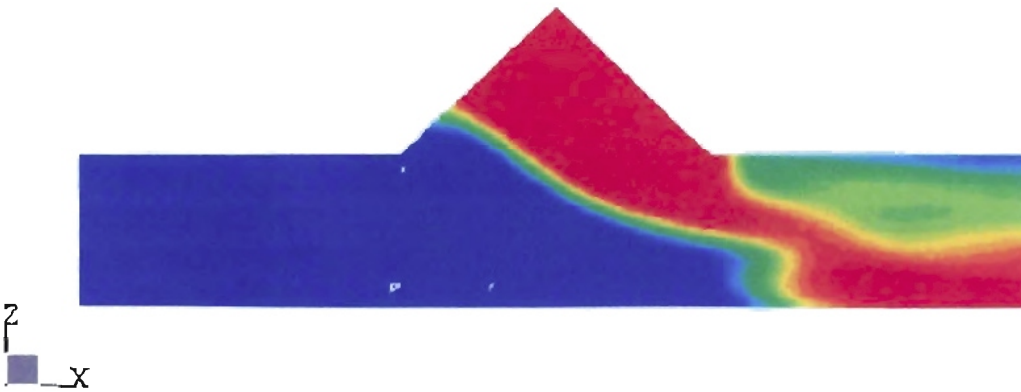


Fig 4-45 Contour plot for tracer distribution at center of the intersection zone (Velocity at Lower Channel inlet=1 m/s and Upper Channel Inlet = 2 m/s)

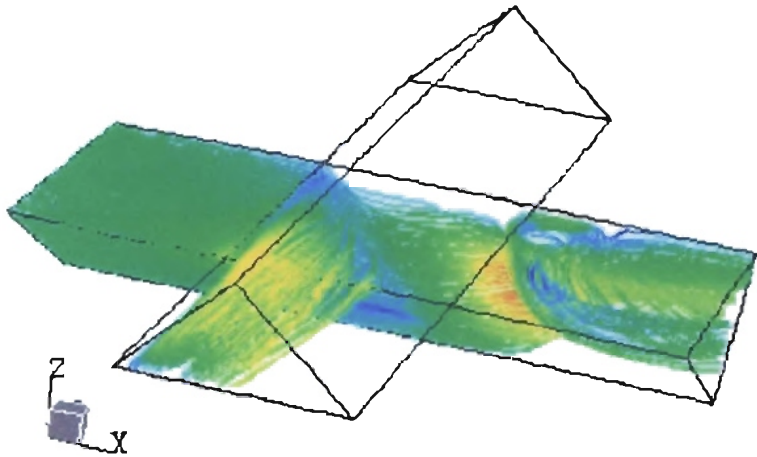


Fig 4-46 Streamline plot for flow entering at Lower Channel inlet (Velocity at Lower Channel inlet=1 m/s and Upper Channel Inlet = 2 m/s)

Velocity at Lower Channel inlet	Splitting Factor
2 m/s (same as Upper Channel)	0.541
1.5 m/s	0.483
2 m/s	0.34

Table 4-4 Variation of Splitting Factor with the velocity specified at Lower Channel inlet

4.5 Large scale simulation

The results discussed so far are obtained for an elementary unit of two adjacent sheets, as shown in Figure 4-4. To study the over all flow pattern in the two-sheet arrangement, geometry was created in CFX-BUILD, as shown in Figure 4-47, with thirty intersecting channels resulting in 110 elementary units. In Figure 4-47, only fifteen channels of top sheet are visible. The adjacent sheet channels (remaining fifteen) are crossing the visible channels in Figure 4-47 at 90°.

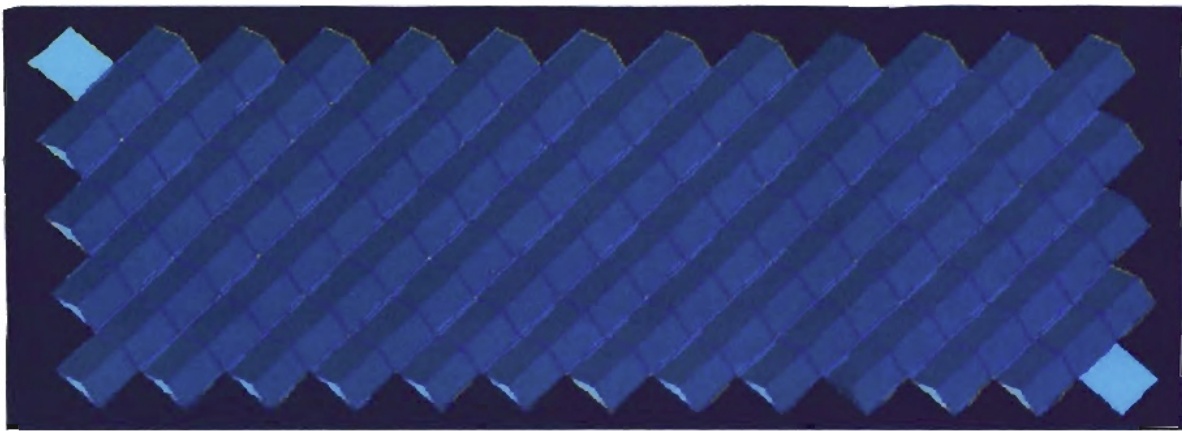


Figure 4-47 Two-sheet geometry with thirty channels (geometry created in CFX-BUILD)

For meshing this geometry with appropriate mesh size, the total number of tetrahedral elements required was 8 million. With the available computational power (Intel Pentium-4, 1.8 GHz, 512 MB RAM processor), it was not possible to perform the simulation for the above mentioned mesh. Therefore, two-sheet geometry with 12 intersecting channels, resulting in 28 elementary units, was studied. The geometry built in CFX-BUILD is shown in Figure 4-48. The channels intersect each other at 90°.

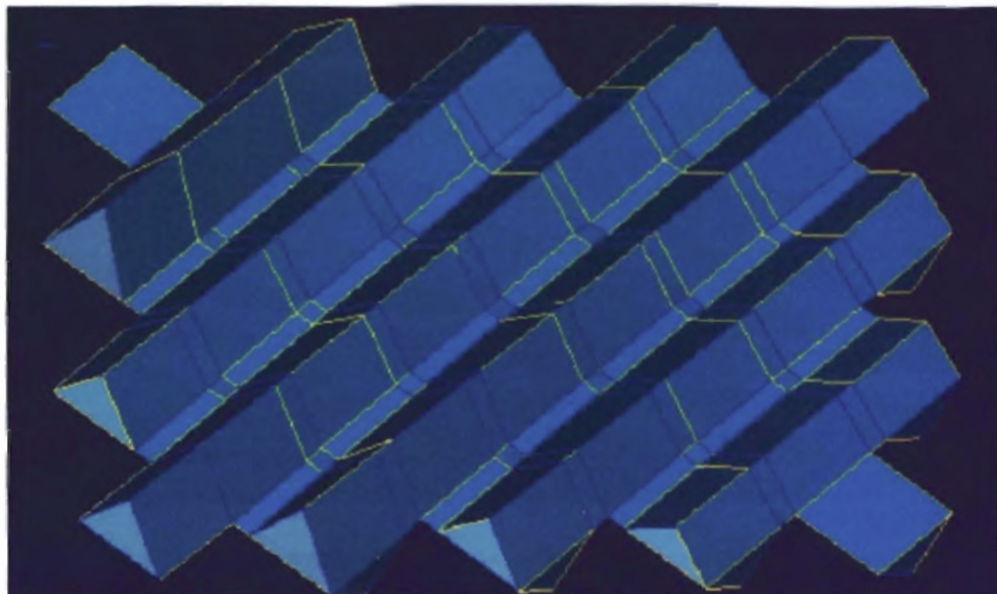


Fig 4-48 Two-sheet geometry with 12 channels i.e. six channels per sheet (geometry created in CFX-BUILD)

4.5.1 Model development

The dimensions of the geometry are shown in Figure 4-49 and 4-50.

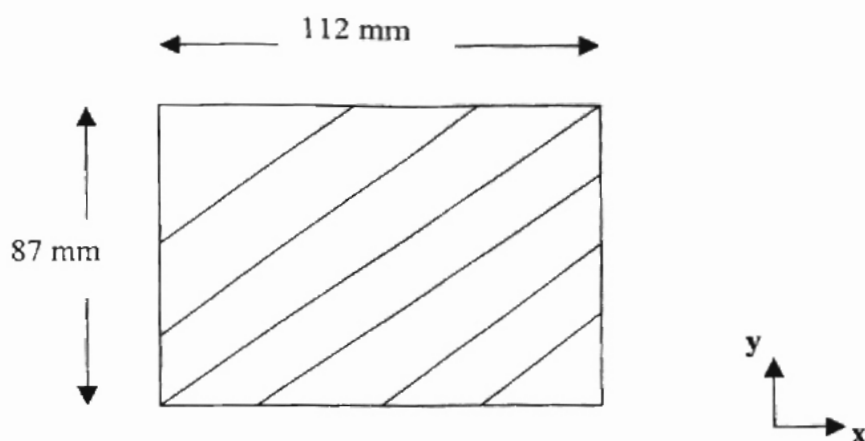


Fig 4-49 Sheet dimensions for the geometry shown in Figure 4-48

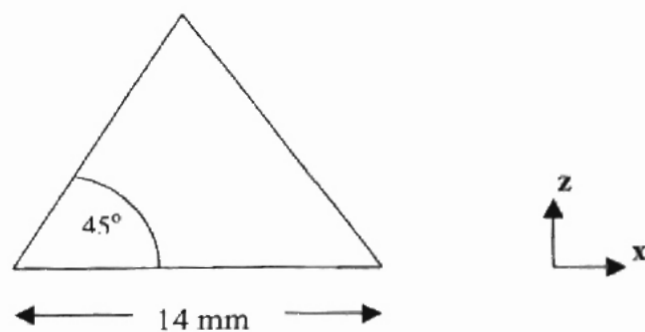


Fig 4-50 Channel cross section for Figure 4-48

There are total eight inlets and eight outlets, four for each sheet. The two sheets are referred to as Upper Sheet and Lower Sheet. To visualize the position of the two sheets, refer to Figure 4-4. The Upper Channel in Figure 4-4 represents the channel positions for Upper Sheet, and Lower Channel for Lower Sheet. Locations of inlet and

outlet boundary conditions are shown in Figure 4-51. The ends of the channels on the right and left side of Figure 4-51 were assumed to be closed, and wall boundary condition was applied there. In Figure 4-51, UI and UO represents inlet and outlet of Upper Sheet channels respectively, and LI and LO represents the same for Lower Sheet. The mathematical models, boundary conditions, and other parameters are same as that of the base case described in section 4.1. Equal velocity was specified for all the inlets with flat velocity profile normal to the surface. The dotted arrows in Figure 4-51 represent the flow direction at the inlets.

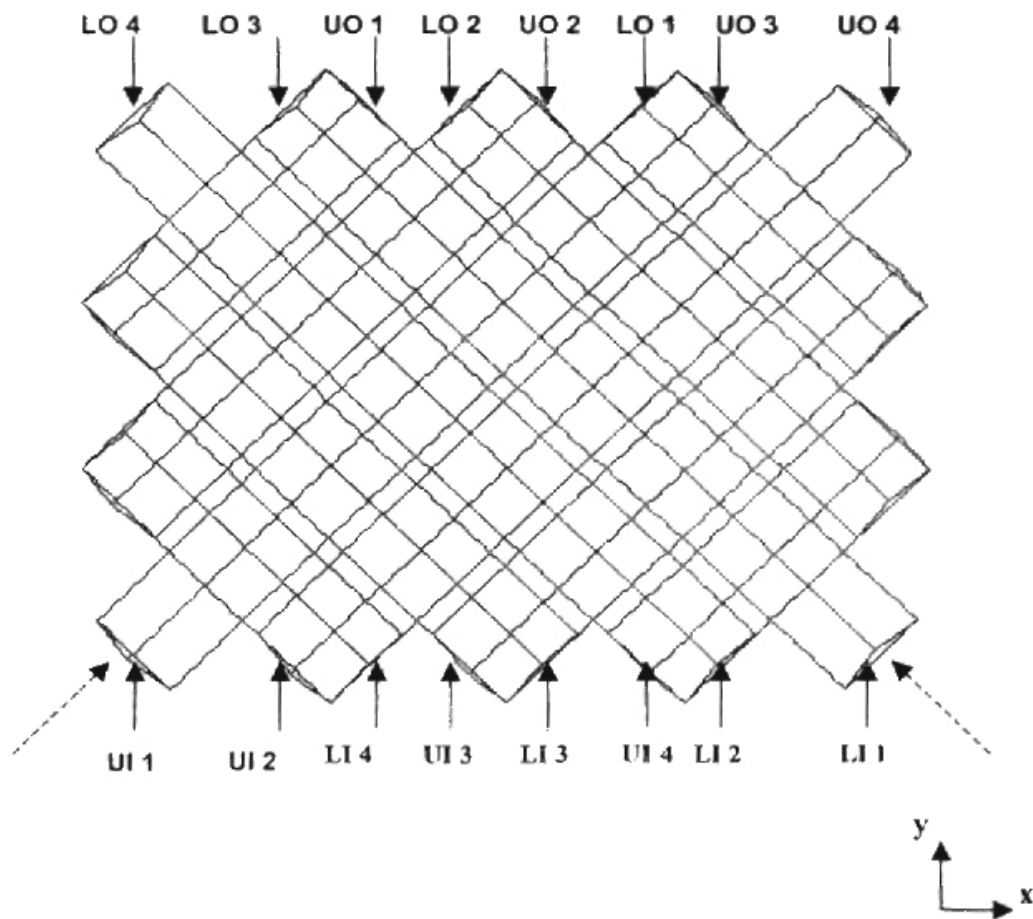


Fig 4-51 Inlet and outlet boundary conditions for two-sheet geometry

4.5.2 Results for large-scale simulation

Qualitative results

Figures 4-52 through 4-59 show the flow path for each inlet. Comparing Figures 4-52 and 4-56, 4-53 and 4-57, 4-54 and 4-58, and 4-55 and 4-59 i.e. similar inlet locations for Upper Sheet and Lower Sheet, it can be observed that the flow pattern is exactly same, but with different orientation. At the side walls, as shown by the circled region in Figures 4-53, 4-54, and 4-55, the flow gets reflected from the walls, and enters the channel of adjacent sheet. From the streamline plots, it can be observed that the criss crossing network of channels, formed between two adjacent sheets, has resulted in considerable radial (x-direction in Figure 4-51) flow distribution.

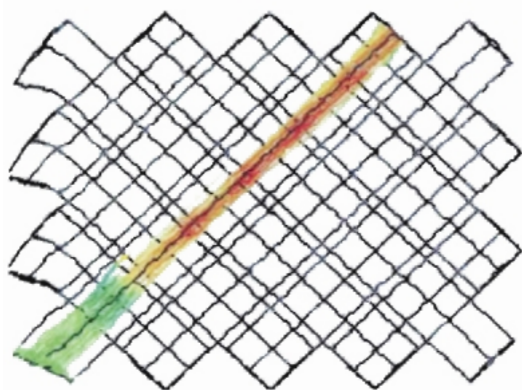


Fig 4-52 Streamline plot for UI 1

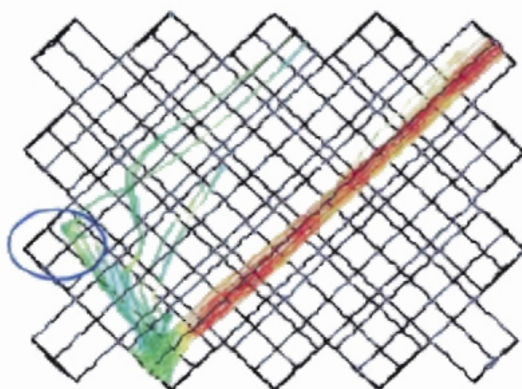


Fig 4-53 Streamline plot for UI 2

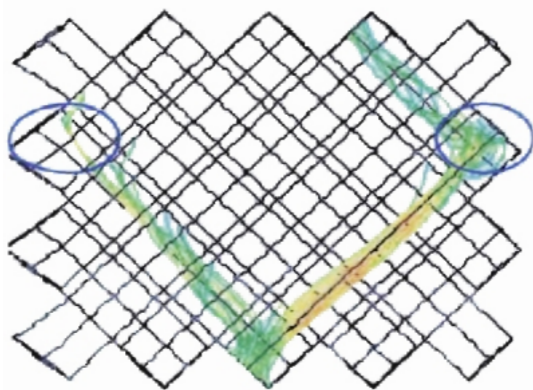


Fig 4-54 Streamline plot for UI 3

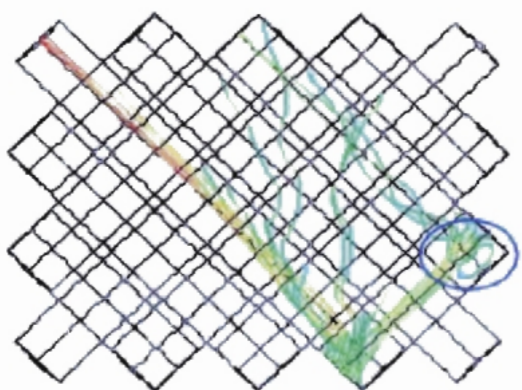


Fig 4-55 Streamline plot for UI 4

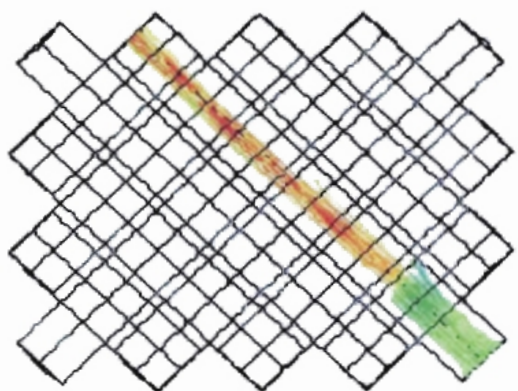


Fig 4-56 Streamline plot for LI 1

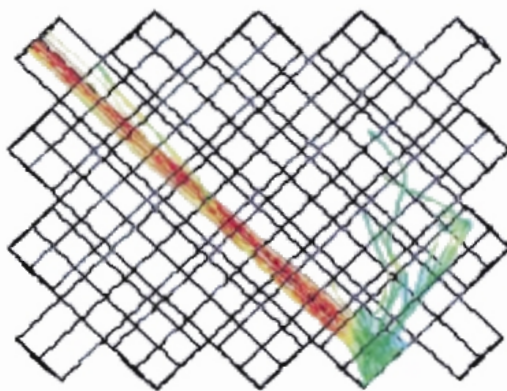


Fig 4-57 Streamline plot for LI 2

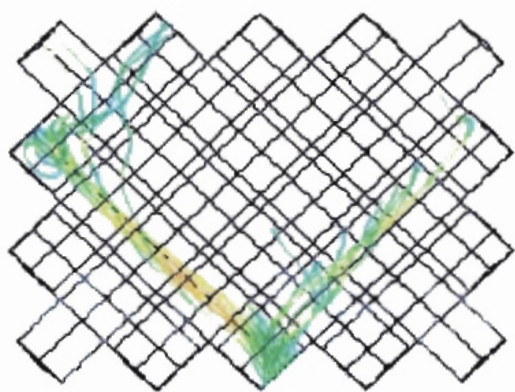


Fig 4-58 Streamline plot for LI 3

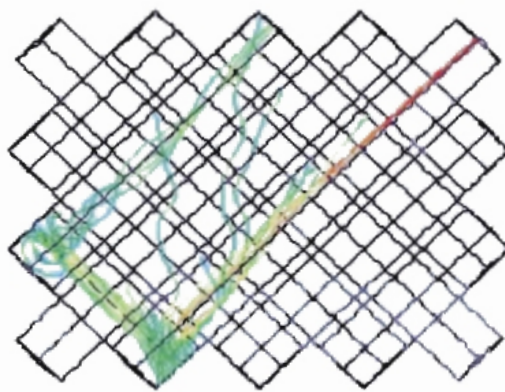


Fig 4-59 Streamline plot for LI 4

Quantitative results

Tracer simulations were conducted to study the flow distribution from a point source i.e. tracer distribution at the outlets when tracer is introduced in only one inlet. Stoter (1993) experimentally studied the tracer distribution in two-sheet system. The experimental results are shown in Figure 4-61. The left and right in Figure 4-61 corresponds to Upper Sheet and Lower Sheet (terms used for adjacent sheets in the CFD simulations) respectively. The experiments were carried out with Montz packing with 17 channels per sheet. The tracer distribution in Figure 4-61 is obtained by introducing tracer at only one inlet location (point source), inlet 16 of right sheet. For the CFD simulation, the tracer was injected at UI 1 (refer Figure 4-51). Experimentally it was observed that most of the tracer is following the channel direction causing a peak at the outlet of the channel in which tracer was introduced (outlet 16 of right sheet in Figure 4-61). The CFD results, shown in Figure 4-60, are in accordance with experimental observations i.e. peak is obtained at UO 3, which represents the channel outlet in which tracer was introduced (UI 1). Tracer mass fraction is almost equal for all the outlets of Lower Sheet. The experiments were carried out with sheets consisting of 17 channels per sheet, whereas there are only four channels per sheet in CFD simulations. If we compare the circled portion in Figure 4-61, which represents four channels, with Figure 4-60, the CFD results corresponding to Upper Sheet qualitatively matches the respective experimental results i.e. right sheet. The decrease in mass fraction for left sheet in Figure 4-61 is quite steep as compared to the Lower Sheet in Figure 4-60.

Comparing Figures 4-52 through 4-55 and 4-56 through 4-59, it is expected that if the tracer is introduced in Lower Sheet at the similar inlet location as that of Upper Sheet, we should get similar tracer distribution as that of Figure 4-60, but with different orientation i.e. the peak for tracer mass fraction should be at LO 3. To verify this, simulations were carried out with tracer injected at LI 1. The tracer distribution is shown in Figure 4-62, which shows similar tracer distribution as that of Figure 4-60, but with different orientation as explained above.

To study the effect of walls, tracer was introduced at UI 4, channel corresponding to which ends at wall. The flow pattern is shown in Figure 4-64 in terms of streamline plot, and tracer distribution is plotted in Figure 4-63. At the intersection zone, shown by circled region in Figure 4-64, the flow gets split, and a part of the flow follows the channel of Upper Sheet (which ends at wall), and remaining flow follows the channel of Lower Sheet (which ends at LO 4). Starting from this intersection zone, to reach LO 4, the flow in the lower channel has to go through five intersection zones; where at each intersection zone the flow will get split. The remaining fraction of the flow from the intersection zone (circled portion) strikes the wall, as highlighted by the rectangular region in Figure 4-64. The flow cannot continue to follow the same channel (because of the wall at the end of the channel), and will be forced to enter the channel of adjacent sheet (which in this case is Lower Sheet).

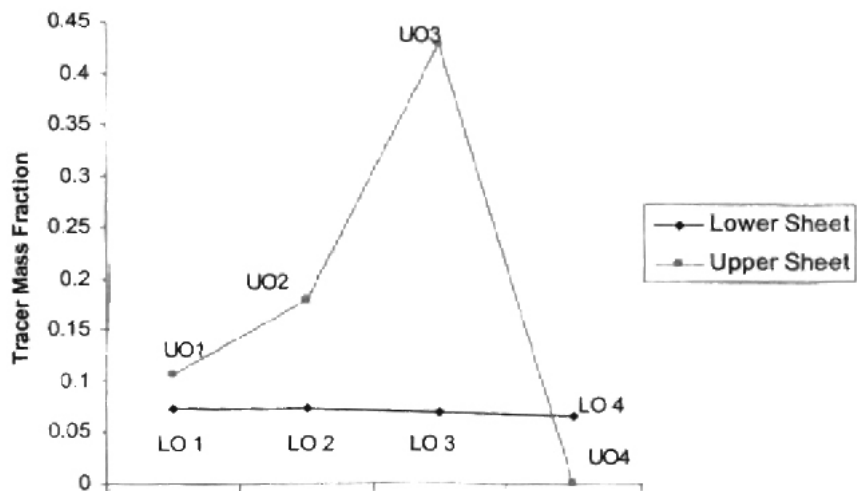


Fig 4-60 Tracer mass fraction distribution with tracer introduced at UI 1

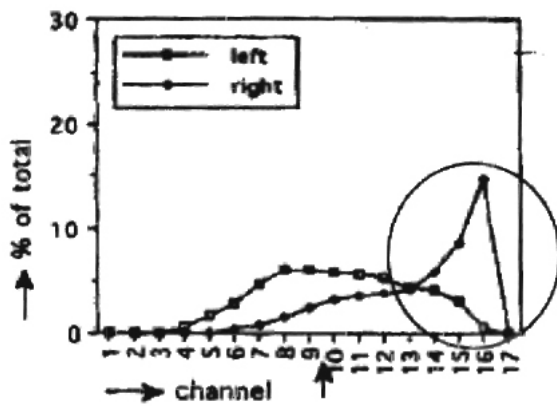


Fig 4-61 Measured tracer distribution in two-sheet system for Montz packing (Stoter, 1993)

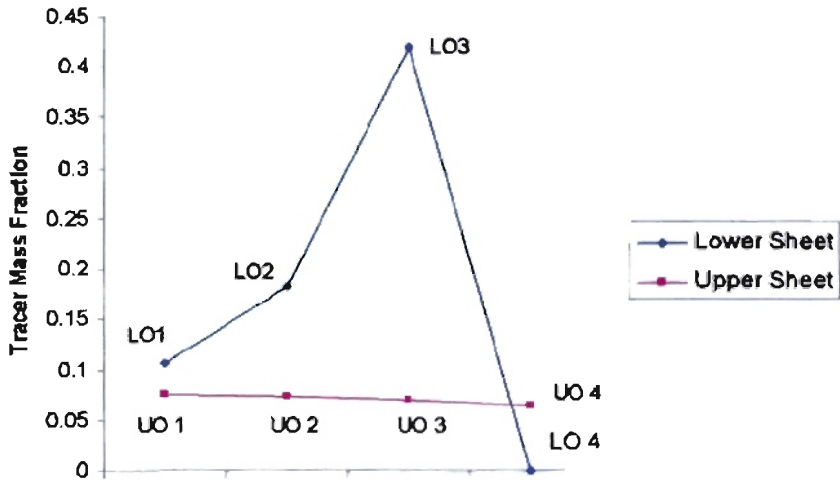


Fig 4-62 Tracer mass fraction distribution with tracer introduced at LI 1

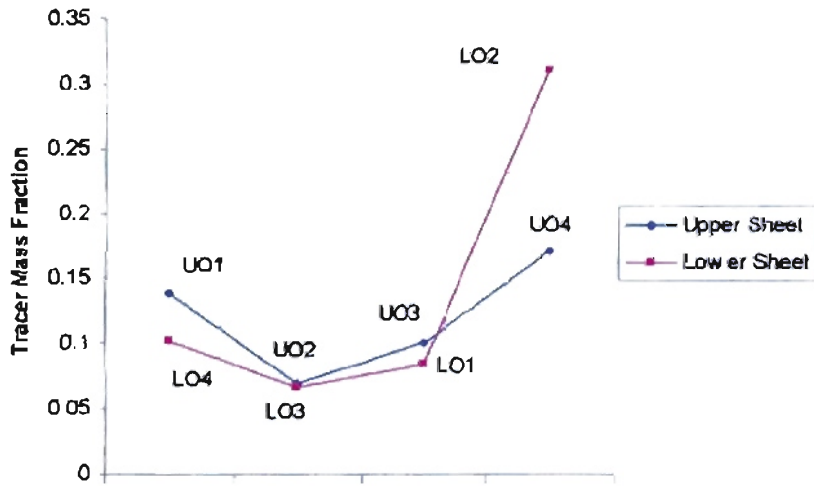


Fig 4-63 Tracer mass fraction distribution with tracer introduced at UI 4

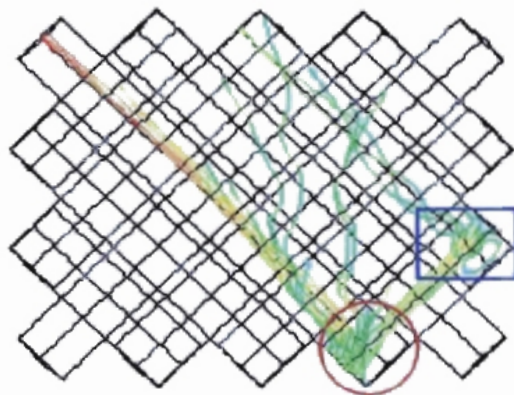


Fig 4-64 Flow pattern for the flow entering at LI 4

CHAPTER 5

CONCLUSIONS AND RECOMMENDATIONS

Currently the structured packing design and development process is purely experimental, and based on experience. The experimental process is carried out by conducting trial and error analysis of the effect of packing design parameters on performance. This process is highly time consuming and uneconomic. The work described in this thesis, based on CFD analysis, will help in reducing the above-mentioned empiricism and the shortcomings associated with it.

5.1 Conclusions

The conclusions derived from the CFD analysis presented in this thesis are:

- Effect of channel intersection on flow distribution in structured packing was studied. Flow gets split at the intersection zone, formed by the channels of the adjacent sheets. A fraction of the flow follows the channel, and rest of the flow enters the channel of adjacent sheet. Therefore, downstream of the intersection zone, mixing of the flow streams from adjacent sheets takes place. Also, this splitting phenomenon results in efficient radial distribution of gas phase in the packed bed. Flow recirculation is expected to develop downstream of the intersection zone, and CFD results were able to capture this effect, at least qualitatively.

- Selection of appropriate Advection Scheme and mesh size is quite crucial in this CFD analysis as shown in Section 4-1. To minimize the errors caused by numerical diffusion in simulations involving flow mixing, use
 - Higher order advection scheme
 - Refined mesh
 - Mesh Adaptation
- Effect of design parameters on packing performance was studied. Pressure drop and Splitting Factor decrease with the increase in channel inclination angle and crimp angle. Splitting Factor is the measure of flow mixing in structured packing bed, and the decrease in the Splitting Factor might result in reduced efficiency for the distillation process. Decrease in pressure drop indicates the increase in packing capacity, and reduction in energy consumption. Therefore, while designing efficient structured packing, a balance between the performance parameters, mentioned above, has to be maintained. Using CFD analysis, design parameters, that need to be tested experimentally, can be short-listed, thereby optimizing the manufacturing process.
- CFD results indicated that wall roughness does not have any effect on Splitting Factor. More study is required to confirm this finding. As expected, pressure drop in case of rough wall is greater than smooth wall, but the difference was not significant.
- The two-sheet CFD analysis showed that the crisscross network of channels results in efficient radial spread of the gas phase.

5.2 Recommendations for future work

The two-sheet system is nothing but repetition of elementary unit cell (as shown in Figure 4-4). Therefore, there is no need of modeling the entire two-sheet system as it is being done in this thesis (Section 4-5). For this type of flow domain, use of periodic boundary conditions is an efficient way of doing CFD analysis. But for the two-sheet system, pressure is not periodic in the flow direction. Therefore, CFX technical support group suggested the use of Customized Periodic Boundary Condition (CPBC). In CPBC, the two-sheet system will be modeled using only one elementary unit cell. Therefore, there will be no need to solve a big mesh (8 million mesh elements), required to mesh the complete geometry of two-sheet system shown in Figure 4-47. Once the solution for one unit cell is obtained, the outlet for that unit cell will act as an inlet for next unit cell. For this data transfer to take place, FORTRAN user routines need to be written. The details about CPBC can be obtained from CFX technical support. Because of the unavailability of FORTRAN Visual-6 compiler (Compiler supported by CFX), no simulation has been carried out using CPBC. Use of CPBC to represent the two-sheet system will not permit to study the effect of sidewalls on flow pattern. To study the effect of walls, complete two-sheet geometry need to be modeled (as being done in this thesis). But, experimental study by Hudson^[12] has shown that the wall effects for gas phase are important only in case of small diameter columns.

Various structured packings (for example, Mellapak) have perforations on the surface. It is believed that since liquid film is present on the surface, the perforations will

not have any effect on the gas flow pattern. But, in case of liquid maldistribution, the perforations will not be covered by liquid. It will be interesting to study the effect of perforations on gas flow pattern. In this thesis, effect of surface roughness on flow pattern is studied. Also, it will be worth studying the entrance effects for the flow transition between structured packing blocks, where the sheets are rotated by 90° from one block to another.

Two-phase CFD model needs to be developed because in reality two phases are present within structured packing. But, the two-phase flow models are not as developed as single-phase models. Therefore, extreme care needs to be taken before drawing any conclusions from the CFD results. The possibility of wrong predictions can be minimized by conducting sensitivity analysis i.e. analyzing the effects of turbulence models, boundary conditions, advection scheme, and mesh size on the CFD results.

Validation of the CFD results is often not given the importance it deserves. Quite often ten-fifteen years old literature data is used for validation of CFD results. But, one should keep in mind that this data was generated for the development/validation of empirical equations, and not for validation of CFD results. In most of the cases, this experimental data gives properties on bulk scale, whereas the purpose of CFD analysis is to study the local phenomena. Therefore, advanced experimental techniques like Computer Tomography, Capacitance Tomography, Doppler Anemometer, and Gamma Ray Scan should be used to build the database suitable for CFD validation.

“CFD and experimentation need to be coupled to establish the credibility of CFD as a design tool”

REFERENCES

- 1) Aroonwilas, A., and Tontiwachwuthikul, P., "Mass Transfer Studies of High Performance structured packing for CO₂ separation Processes" *Energy Conservs. Mgmt.* Vol. 38, Suppl. P S75-S80, 1997
- 2) Bakker, A., Haidari, A. H. and Oshinowo, L. M., "Realize Greater Benefits from CFD," *Chem. Eng. Prog.* Vol. 97, No.3, p. 45-53, 200f
- 3) Carmen Rey, M., Glasserman, P., Bohm, U., "Mass Transfer to Regular Packings at Low Reynolds Numbers and under Natural Convection" *Int. J. Heat Mass Transfer*, Vol. 41, No. 12, p 1693-1706, 1998
- 4) Edwards, D. P., Krishnamurthy, K. R., Potthoff, R. w., "Development of an Improved Method to quantify Maldistribution and its Effect on Structured packing Column Performance" *Trans IchemE*, Vol. 77, Part A, October 1999
- 5) Fair, J. R., and Bravo, J. L., "Distillation Columns Containing Structured Packing" *Chemical Engineering Progress*, p 19-29, January 1990
- 6) Fair, J. R., Nicolaiewsky, E. M. A., Tavares, F. W., Rajagopal, K., "Liquid Film flow and Area Generation in Structured Packed Columns" *Powder Technology*, Vol. 104, p 84-94, 1999
- 7) Fair, J.R., Seibert, F. A., Behrens, M., Saraber, P. P., Olujić, Z., "Structured Packing performance-Experimental Evaluation of Two Predictive Models" *Ind. Eng. Chem. Res.*, Vol. 39, p 1788-1796, 2000
- 8) Gaiser, G. and Kottke, V., "Flow Phenomena and Local Heat and Mass Transfer in Corrugated Passages" *Chem. Eng. Technology*, Vol. 12, p 400-405, 1989
- 9) Gulijik, C., "Using Computational Fluid Dynamics to Calculate Transversal Dispersion in Structured Packed Bed" *Computers Chem. Engg.*, Vol. 22, Suppl. P S767-S770, 1998
- 10) Hanley, B., Dunbobbin B., Bennett, D., "A Unified Model for Countercurrent Vapor/Liquid Packed Columns. 1. Pressure Drop" *Ind. Eng. Chem. Res.*, Vol. 33, p 1208-1221, 1994

- 11) Hanley, B., Dunbobbin B., Bennett, D., "A Unified Model for Countercurrent Vapor/Liquid Packed Columns. 2. Equation for the Mass-Transfer Coefficients, Mass-Transfer Area, the HETP, and the Dynamic Liquid Holdup " *Ind. Eng. Chem. Res.*, Vol. 33, p 1222-1230, 1994
- 12) Hodson, J. S., Fletcher, J. P., Porter, K. E., "Fluid Mechanical studies of Structured Distillation Packings" *JchemE*, Vol. 142, p 999-1007, 1997
- 13) Iliuta, I., and Larachi, F., "Mechanistic Model for Structured-Packing-Containing Columns: Irrigated Pressure Drop, Liquid Holdup, and Packing Fractional Wetted Area" *Ind. Eng. Chem. Res.*, Vol. 40, p 5140-5146, 2001
- 14) Jiang, Y., Khadilkar, M. R., Al-Dahhan, M. H., Dudukovic, M. P., "CFD Modeling of Multiphase Flow Distribution in Catalytic Packed Bed Reactors: Scale Down Issues" *Catalysis Today*, Vol. 66, p 209-218, 2001
- 15) Kister, H. Z., "Distillation Design", McGraw-Hill, Inc., 1992
- 16) Krishna, R., van Baten, J. M., Ellenberger, J., "Radial and Axial Dispersion of the Liquid Phase Within a KATAPAK-S[®] Structure: Experiments vs. CFD Simulations" *Chem. Eng. Sci.*, Vol. 56, No. 3, p 813-821, 2001
- 17) Logtenberg, S. A., and Dixon, G. A., "Computational Fluid Dynamics Studies of Fixed Bed Heat Transfer" *Chemical Engineering Progress*, Vol. 37, p 7-21, 1998
- 18) Loser, T., Petritsch, G., Mewes, D., "Investigation of Two-Phase Countercurrent Flow in Structured Packing Using Capacitance Tomography" 1st World Congress on Industrial process Tomography, Buxton, Greater Manchester, April 14-17, p 354-361, 1999
- 19) Mohamed, A. a., Jansens, P., Olujic, Z., "CFD Simulation Software- A Design Tool for Packed Column Internals?" Topical Conference on Distillation Tools for the Practicing Engineer, AIChE Spring Meeting, New Orleans, March 10-14, 2002
- 20) Mohamed, A. a., Jansens, P., Olujic, Z., "CFD Simulation Software- A Design Tool for Packed Column Internals?" Topical Conference on Distillation Tools for the Practicing Engineer, AIChE Spring Meeting, New Orleans, March 10-14, 2002
- 21) Nandakumar, K., Yin, F. H., Sun, C. G., Afacan, A., Chuang, K. T., "CFD Modeling of Mass-Transfer processes in Randomly Packed Distillation Columns" *Ind. Eng. Chem. Res.*, Vol. 39, p 1369-1380, 2000
- 22) Olujic, Z., Seibert, A. F., Fair, J. R., "Influence of Corrugation Geometry on the Performance of Structured Packings: An Experimental Study" *Chemical engineering and Processing*, Vol. 39, p 335-342, 2000

- 23) Olujic, Z., and de Graauw, J., "Appearance of Maldistribution in Distillation Columns Equipped with High Performance Packing" *Chem. Biochem. Eng. Q*, Vol. 3, No. 4, p 181-196, 1989
- 24) Parsons, I. M. and Porter, K. E., "Gas Flow Patterns in Packed Beds: A Computational Fluid Dynamics Model for Wholly Packed Domains" *Gas Separation and Purification*, Vol. 6, No. 4, 1992
- 25) Petre, C. F., Larachi, F., Iliuta, I., Grandjean, B. P. A., "Pressure Drop Through Structured Packings: Breakdown into the contributing mechanisms by CFD modeling" *Chem. Eng. Sci.*, Vol. 58, p 163-177, 2003
- 26) Porter, K. E., "Why Research is Needed in Distillation," *Trans. IChemE.* , Vol. 73, part A, p 357-362, 1995
- 27) Rocha, J. A., Bravo, J. L., Fair, J. R., "Distillation Columns Containing Structured Packings: A Comprehensive Model for their Performance. I. Hydraulic Models" *Ind. Eng. Chem. Res.*, Vol. 32, p 641-651, 1993
- 28) Shetty, S. and Cerro, L., R., "Fundamental Liquid Flow Correlations for the Computation of Design Parameters for Ordered Packings" *Ind. Eng. Chem. Res.*, Vol. 36, p 771-783, 1997
- 29) Speziale, C. G., "Analytical Methods for the Development of Reynolds-Stress Closures in Turbulence" *Annu. Rev. Fluid Mech.*, Vol. 23, p 107-157, 1991
- 30) Spiegel, L., Bomio, P., Hunkeler, R., "Direct Heat and Mass Transfer in structured Packings" *Chemical Engineering and Processing*, Vol. 35, p 479-485, 1996
- 31) Stichlmair, J. G. and Fair, J. R., "DISTILLATION Principles and Practice" Wiley-VCH, 1998
- 32) Stoter, F., Olujic, Z., de Graauw, J., "Modeling and Measurement of Gas Flow Distribution in Corrugated Sheet structured Packings" *The Chemical Engineering J.*, Vol. 53, p 55-66, 1993
- 33) Stoter, C.F., "Modeling of Maldistribution in Structured Packings: From Detail to Column Design", Ph.D. Thesis, Delft University, 1993
- 34) Umeda, S., Yang, W., Tanaka, T., "Mechanics and Correlations of Flow Phenomena in Intersecting Ducts" *Experiments in Fluids*, Vol. 17, p 323-329, 1994
- 35) Versteeg, H. K. and Malalasekera, W. "An Introduction to Computational Fluid Dynamics: The Finite Volume Method" Prentice Hall, 1995

- 36) Xu, Z. P., Afacan, A., Chuang, K. T., "Predicting Mass Transfer in Packed Columns Containing Structured Packings" *Trans IchemE*, Vol. 78, Part A, p 91-98, January 2000
- 37) Zhang, N., Yang, W., Lee, C. P., "Heat Transfer and Friction Loss Performance in Flow Networks with Multiple Intersections" *Experimental Heat Transfer*, Vol. 6, p 243-257, 1993
- 38) Zuiderweg, F. J., Kunesh, J. G., King, D. W., "A Model for the calculation of the Effect of Maldistribution on the Efficiency of a Packed Column" *Trans IchemE*, Vol. 71, Part A, p 38-44, January 1993
- 39) <http://www.cfdreview.com/features/01/04/28/2131215.shtml>, 03/26/2003
- 40) <http://www.grc.nasa.gov/WWW/wind/valid/archive.html>, 03/26/2003
- 41) CFX-5.5.1. User Manual

2.

VITA

Swapnil Y. Dhumal

Candidate for the Degree of

Master of Science

Thesis: STUDY OF SINGLE-PHASE FLOW IN STRUCTURED PACKING USING
COMPUTATIONAL DYNAMICS

Major Field: Chemical Engineering

Biographical:

Personal Data: Born in Maharashtra, India, on May 22, 1980, the son of Yashwant
and Surekha Dhumal

Education: Graduated from Shri Shivaji Science College, Nagpur, Maharashtra,
India in July 1997; received Bachelor of Technology degree in
Chemical Engineering from Laxminarayan Institute of Technology,
Nagpur, Maharashtra, India in July 2001. Completed the requirements
for the Master of Science degree with a major in Chemical
Engineering at Oklahoma State University in August 2003.